Journal of Magnetic Resonance 300 (2019) 61–75

Contents lists available at ScienceDirect

Journal of Magnetic Resonance

journal homepage: www.elsevier.com/locate/jmr

Polarization recovery during ASAP and SOFAST/ALSOFAST-type experiments

Martin R.M. Koos *, Burkhard Luy

Institute of Organic Chemistry and Institute for Biological Interfaces 4, Karlsruhe Institute of Technology (KIT), Hermann-von-Helmholtz-Platz 1, 76344 Eggenstein-Leopoldshafen, Germany

ARTICLE INFO

Article history:
Received 24 September 2018
Revised 3 December 2018
Accepted 15 December 2018
Available online 17 December 2018

Keywords:
ASAP-HSQC
ASAP
ALSOFAST
Small molecules
Steady state
Variable flip angle
Relaxation

ABSTRACT

Experiments with fast repetition schemes significantly enhance the capabilities of modern NMR spectroscopy. Two schemes for heteronuclear correlation experiments that have been presented are the ASAP and the ALSOFAST method. The first method is Acceleration by Sharing Adjacent Polarization (ASAP) for samples at natural abundance isotope level. It was originally derived in the ASAP-HMQC and recently received renewed attention in the ASAP-HSQC. Sharing the polarization of active protons with the surrounding reservoir can result in seemingly instant polarization recovery and therefore enormous gains in sensitivity, but can also lead to a slight reduction of polarization and spectral intensity, depending on sample and setup. A second type of setup has been introduced with the so-called Alternate SOFAST (ALSOFAST-) HMQC and ALSOFAST-HSQC for natural abundance $^{1}H,^{13}C$-correlation experiments and in the SOFAST-HMQC for $^{1}H,^{15}N$-correlations. In these cases, the reservoir spins are only maintained through the pulse sequence without Hartmann-Hahn-type mixing. A model for the estimation of the available polarization in the fast repetition schemes could be a valuable tool for experimentalists and pulse sequence developers.

Starting from the well-known Ernst angle model, we derive in this article several mathematical models that describe the polarization over the course of ALSOFAST and ASAP type experiments. The models can be used to visualize the initial scans of an experiment and even more importantly, show the polarization and achievable signal intensity in the steady state of an experiment. In this way the two extreme applications of ASAP- and ALSOFAST-type acquisition schemes are covered: (i) acquisition using progressive excitation for experiments with few increments and shortest possible overall acquisition times and (ii) steady-state-type experiments with ultrahigh resolution and correspondingly large number of increments. The two resulting excitation strategies are applied to maximize SNR in different situations. To test the models, experimental data was obtained by special pulse sequences and examples are shown for different spin environments. The results show good agreement between theory and experiment.

1. Introduction

The acceleration of the acquisition of NMR spectra is an ongoing effort reaching back into early days of the method. One of the first treatises is the optimal combination of interscan recovery delay and excitation angle in simple pulse-acquire experiments, resulting in the well-known Ernst angle to maximize signal-to-noise ratio (SNR) [1–3]. Its implementation in magnetic resonance imaging (MRI) in the Fast Low-Angle Shot (FLASH) method brought a revolutionary speed-up [4,5], enabling e.g., the real time 3D image acquisition of a beating human heart [6]. It is also available in many fast heteronuclear methods including the Band-Selective Optimized Flip-Angle Short-Transient (SOFAST-) HMQC and the Alternate SOFAST (ALSOFAST-) approach [7–10].

A fundamentally new method introduced MRI concepts into NMR: *Ultrafast* (UF) experiments utilize spatially resolved acquisition to obtain a full 2D spectrum in a single scan [11–14]. If SNR is sufficient, this method requires no interscan polarization recovery and therefore provides ideal time resolution and is especially well-suited for hyperpolarized samples where polarization does not recover to initial values. There are severe limits in accessible resolution and spectral width due to diffusion and available gradient strengths and switching times, but the scheme has been combined with many of the classical NMR experiments [15–19]. Other approaches include artifact suppression after drastic reduction of

* Corresponding author.
E-mail address: martin.koos@kit.edu (M.R.M. Koos).

https://doi.org/10.1016/j.jmr.2018.12.014
1090-7807/

interscan recovery delays [20,21] or methods that allow acquisition of a reduced data set by applying special processing techniques [22–27].

An advanced method is the acceleration of polarization recovery between scans, allowing reduced interscan recovery delays without corresponding loss of polarization recovery. This can be achieved by band-selective spin manipulation, e.g. in the SOFAST, Band-Selective Excitation Short-Transient (BEST) and Cooling Overall Spin Temperature (COST) experiments [7,8,28–30], especially suited for proteins, or by taking advantage of the INEPT step and utilize it to selectively address non-^{13}C-bound protons like in the ALSOFAST and ASAP experiments at natural isotope abundance [10,31–33]. In all these cases, a subset of the spins is treated as reservoir which is arranged to be in equilibrium state at the end of the sequence. The reservoir can then provide additional polarization by chemical exchange if the solvent is protonated and part of the reservoir [28,29], by NOE if sign and magnitude of corresponding cross relaxation terms allow it [9,10], or by active mixing of magnetization using an RF pulse sequence like in the ASAP methods covered in this work [10,31].

Two situations represent the main application of fast sequences and will be addressed in the following: the limit of extremely short experiments with 2D acquisition times as low as few seconds and the steady-state-limit for 2D acquisition with extreme resolution in the indirect dimension. We first repeat the models for the Ernst angle in the fast and steady-state limits and then derive corresponding models for ALSOFAST- and ASAP-HSQC-type experiments. We then compare the results with each other and with conventional HSQC experiments in terms of sensitivity. In addition, we compare selected results with experimental data.

2. Theory

In most modern NMR experiments, the sample is solely polarized by the external magnetic field before a defined sequence of pulses is applied followed by the acquisition of the free induction decay (FID) [1,34]. Usually, the pulse sequence is repeated a number of times for various reasons, and the acquired signals of individual scans are combined.

When only a single pulse is applied per repetition, the effective flip angle of the RF pulse together with relaxation properties of interacting spins determine signal intensities and polarization recovery in between scans. Fig. 1A shows the effect of repeated 90° pulses and repetition times shorter than T_1 on the polarization. While the first pulse creates a large signal, the polarization does not recover and all subsequent pulses create constant but small signal intensities. The effect can be circumvented by increasing acquisition times τ_{acq} and/or including an additional delay. The additional delay is called d_R and should not be confused with the full length of the relaxation period $\tau_{rec} = \tau_{acq} + d_R$. In addition, the length of one repetition of the experiment is called T_R in this work.

While a 90° pulse provides maximum intensity for a single scan, in many cases it is advantageous to use a lower effective flip angle and reduce the extra delay d_R to increase the overall SNR from repeated scans. In Fig. 1B, the effect of reducing the flip angle is visible: incomplete excitation retains part of the polarization, but the signal intensity is low compared to 90° excitation. After some repetitions, however, a steady state of polarization depletion and recovery is reached. This steady state may result in *higher* signal intensity than the intensity achieved with repeated 90° pulses [3].

The flip angle yielding maximum SNR for a certain set of T_1 and τ_{rec} times has long been known and is called the Ernst angle [1–3]. Ernst angle excitation or an approximation thereof is commonly utilized for compatible pulse sequences in NMR spectroscopy.

It has been shown that the SNR of an experiment also depends on the ratio of acquisition time τ_{acq} to T_2 time [1–3]. For a simple pulse-acquire experiment on a small molecule with $T_1 \approx T_2$, maximum SNR is achieved with $T_R \approx 1.3 \cdot T_1$ and $\tau_{acq} = T_R$ (and $\beta_{opt} = 74°$). In HSQC-type experiments, the length of τ_{acq} is usually limited by the allowed decoupling duration and $\tau_{acq} < T_R$. Furthermore, the required resolution and therefore τ_{acq} in practice (and in this work) generally does not change significantly for HSQC experiments. The contribution of resolution is therefore assumed to be constant for all experiments and τ_{acq}/T_2 is not included in the model. In all cases, of course, $\tau_{acq} \leqslant \tau_{rec} < T_R$ has to be fulfilled.

As seen in Fig. 1B, the signal intensity of the first few scans is transient. In many cases, e.g. when the same amount of polarization per increment is needed, these FIDs are discarded by recording so-called dummy scans. An alternative to using a constant flip angle to reach constant signal intensity in the steady state of a repetitive experiment, is to use varying flip angles to achieve constant signal amplitude. Especially for experiments with very short durations, a sequence of flip angles can be advantageous as has been shown for imaging applications as well as hyperpolarized samples [35–38]. This approach is also reflected as "progressive excitation" at the end of the theory section and the last part of this article.

2.1. Ernst angle model: steady state

The Ernst angle is the flip angle providing maximum steady state SNR for a combination of recovery delay τ_{rec} and relaxation

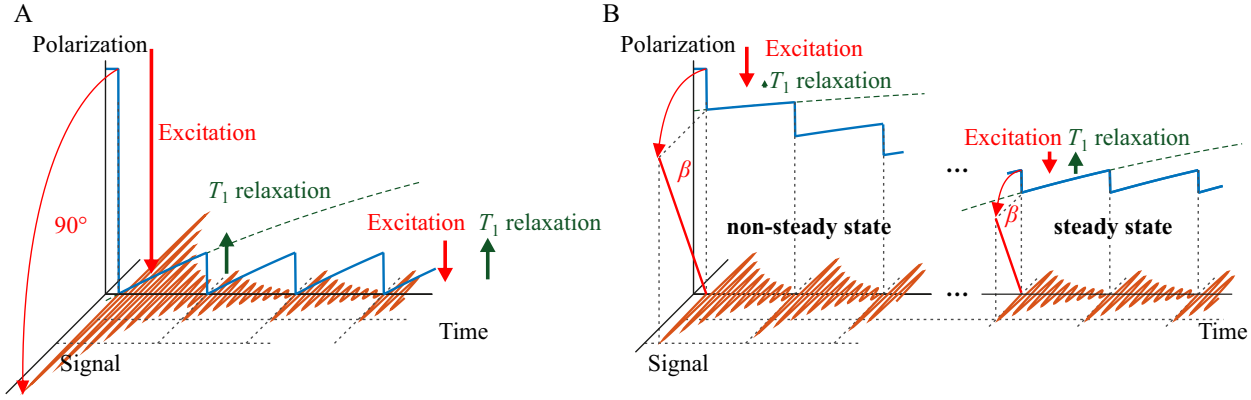

Fig. 1. Polarization under the effect of repeated excitation pulses. Excitation pulses reduce polarization by an amount dependent on the *current* polarization, while recovery is dependent on the currently *missing* polarization (difference between actual polarization and equilibrium polarization). After a number of repetitions, the two effects equilibrate and a steady state arises ($\tau_{rec} = 0.2T_1$). (A) Case of 90° excitation and insufficient recovery between scans. (B) Ernst angle case with β-pulse excitation.

time T_1. It was introduced for a model pulse sequence as shown in Fig. 2A. While Fig. 1 is focused on the steady state polarization, Fig. 2B and C shows the steady state signal intensity more accurately. The signal intensity depends on $M_z \cdot \sin(\beta)$ for maximum steady state signal intensity, a balance between the two factors has to be found.

Starting with the polarization $M_z(0)$, after a pulse with flip angle β the polarization

$$M_z(0_+) = M_z(0)\cos(\beta) \tag{1}$$

is retained. After the pulse, T_1 relaxation will recreate polarization during a time $\tau_{rec} \approx T_R$. Right before the next pulse, magnetization has recovered to

$$M_z(T_R) = M_z(0_+) + (M_0 - M_z(0_+)) \cdot (1 - E_1) \tag{2}$$

with

$$E_1 = \exp(-\tau_{rec}/T_1). \tag{3}$$

In the steady state

$$M_z(T_R) = M_z(0), \tag{4}$$

therefore

$$M_z(0) = M_0 \frac{1 - E_1}{1 - E_1\cos(\beta)} \tag{5}$$

and the initial amplitude of the FID, $M_x(0_+)$ is

$$M_x(0_+) = M_0 \frac{1 - E_1}{1 - E_1\cos\beta}\sin(\beta). \tag{6}$$

The maximum signal amplitude is obtained for

$$\cos(\beta_{opt}) = E_1, \tag{7}$$

the original definition of the Ernst angle [1–3].

2.2. Conventional HSQC in the steady state

The well-known HSQC experiment in its conventional form does not allow Ernst angle excitation. The magnetization transfer via INEPT requires 90° pulses, untransferred magnetization can contribute to artifact signals and is therefore dephased to prevent detection or removed by pulse phase cycling. In the conventional HSQC the INEPT element is always matched to a single $^1J_{CH}$ coupling constant, so that in real samples a compromise has to be made. While ideas for J-compensated transfer exist [39–41], these have not been included in any of the fast HSQC methods so far.

The model of a more general pulse sequence, e.g. a conventional HSQC, is shown in Fig. 3A. The duration τ_{seq} and the different effects of the sequence on magnetization pathways have to be considered. Each scan features complete excitation, indicated by the 90° excitation pulse. The full excitation leaves no polarization reservoir, i.e., $M_z(\tau_{seq}) = 0$. The steady state polarization after the excitation pulse is therefore equal to the single scan polarization after the initial pulse

$$M_z(0) = M_0(1 - E_1). \tag{8}$$

The combined effects of polarization losses due to the pulses of the pulse sequence, relaxation, transfer mismatch and other parameters have to be considered in addition to the simple 1D experiment. This is most easily achieved by introducing an empirical factor that depends on the particular spin system and spectrometer settings, i.e. $E_{seq} = E_{seq}(T_1, T_2, t_1, \nu_{off}, {}^1J_{CH}, J_{HH}, \ldots)$. Such a parameter can best be determined experimentally. This factor will

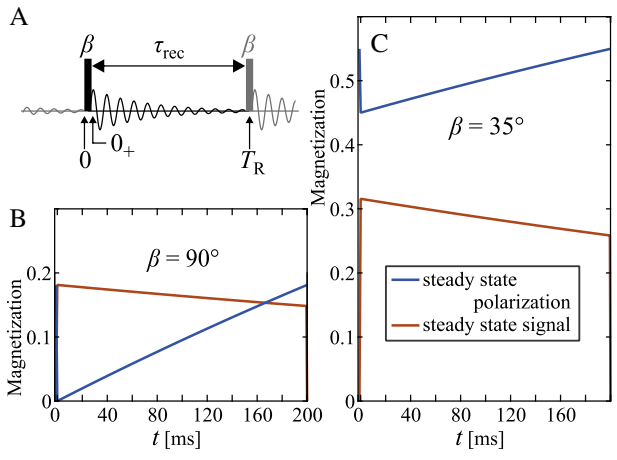

Fig. 2. (A) Ernst angle model, pulse sequence and time definitions. The nomenclature follows Ernst et al. [3]. At time 0 the sequence starts with a β-pulse before the acquisition starts at time 0_+. With the FID the polarization starts to recover during τ_{rec} and the experiment is repeated after T_R. (B) Steady-state polarization and signal with full excitation, $\beta = 90°$, for the case $T_1 = T_2 = 1$ s. (C) Steady-state polarization and signal with Ernst angle excitation, $\beta = 35° \approx \beta_{opt}$, for the same time constants.

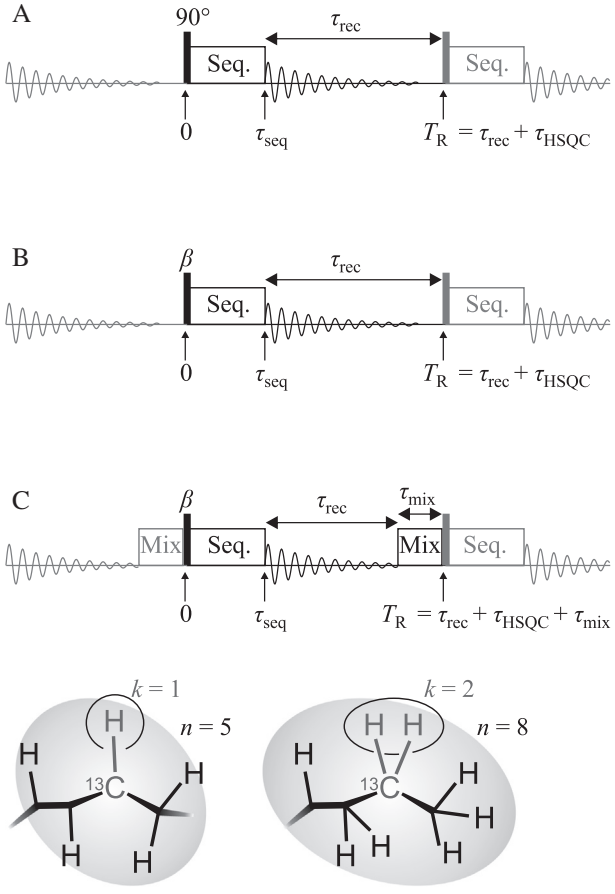

Fig. 3. Pulse sequence models for calculations of the three HSQC experiments used in this work. The experiments start at $t = 0$ with β excitation within an HSQC sequence. The HSQC pulse sequence ends at $t = \tau_{seq}$, which would be the start of the FID in a normal experiment. Acquisition duration and a possible additional delay is combined in the recovery delay τ_{rec}. Before the next scan, a mixing block of length τ_{mix} is included in the ASAP-HSQC (C). The next scan starts at the repetition time $t = T_R$. Typical values are $\tau_{seq} = 10$ ms and $\tau_{mix} = 35$ ms with τ_{rec} in the range of 100 ms to seconds. (A) Conventional HSQC with full excitation, no reservoir magnetization. (B) ALSOFAST-HSQC; optimized excitation preserves reservoir magnetization. (C) ASAP-HSQC; optimized excitation to preserve reservoir magnetization and averaging of active and remote spins by a mixing sequence. In the bottom, two example spin systems are shown with $k = 1, n = 5$ and $k = 2, n = 8$, respectively, as further explained in Section 2.4.

also differ for different coherence transfer pathways, therefore E_{seq} is used in the following for the effect on final polarization, i.e. the reservoir, and E^*_{seq} is used for the effect on polarization that is converted to coherence for detection. Out of the two, only the reservoir parameter E_{seq} is affecting the steady state. In a conventional HSQC experiment, all unused magnetization is dephased and $E_{seq} = 0$. The situation is different for the ALSOFAST and ASAP variants as discussed below.

2.3. Steady state for ALSOFAST-type experiments

The ALSOFAST-HSQC sequence retains unused magnetization along z. Conservation of the reservoir allows an Ernst angle excitation scheme to increase repetition rate and signal intensity, as shown in Fig. 3B. Partial excitation as an equivalent to the Ernst angle β can be achieved by incomplete transfer during the initial INEPT step [10].

For determining optimal excitation, the loss of magnetization due to relaxation, incomplete coherence transfer and pulse imperfections during the experiment need to be taken into account, which is again accomplished by an empirical factor $E_{seq}(T_1, T_2, t_1, \nu_{off}, {}^1J_{CH}, J_{HH}, \ldots)$. For simplification, a single factor E_{seq} is considered for the polarization in the following.

A layout of the acquisition scheme with contributing factors is shown in Fig. 3B. Compared to the simple pulse-acquire scheme in Fig. 2A, the excitation with the Ernst angle is combined with loss of polarization according to E_{seq}, resulting in

$$M_z(\tau_{seq}) = M_z(0)\cos(\beta)\cdot E_{seq}. \tag{9}$$

After the pulse sequence, during acquisition and during the recovery delay, the polarization recovers starting at $t = \tau_{seq}$ until the start of the next scan at $T_R = \tau_{seq} + \tau_{rec}$. The recovery due to T_1 relaxation leads to

$$M_z(T_R) = M_z(\tau_{seq})E_1 + M_0(1 - E_1) \tag{10}$$

and with the steady state condition

$$M_z(T_R) = M_z(0)$$

this results in the steady state polarization

$$M_z^{ALSO}(0) = \frac{M_0(1 - E_1)}{1 - E_{seq}E_1\cos(\beta)}. \tag{11}$$

The corresponding signal intensity is then given by

$$M_x^{ALSO}(\tau_{seq}) = \frac{M_0(1 - E_1)}{1 - E_{seq}E_1\cos(\beta)}\cdot E^*_{seq}\sin(\beta), \tag{12}$$

including losses of detected coherences during the pulse sequence as described empirically by E^*_{seq}. Optimal excitation in the ALSOFAST-HSQC is achieved with

$$\cos(\beta^{ALSO}_{opt}) = E_{seq}E_1, \tag{13}$$

an expression very similar to the original Ernst angle formula. Both E_1 and E_{seq} may vary significantly within a sample, rendering the experimentalist to approximate settings.

2.4. Steady state of ASAP experiments

In the case of the ASAP-HSQC, the situation is more complicated as additional contributions from surrounding spins need to be taken into account. The ASAP-HSQC, as outlined in Fig. 3C, is very similar to the ALSOFAST-HSQC but includes an additional mixing block, typically isotropic mixing by a TOCSY multiple pulse sequence like DIPSI-2 [42], FLOPSY [43], or MOCCA-XY16 [44–46]. Due to the mixing period, the spin reservoir with potentially differing relaxation properties needs to be considered. It also requires separate, parallel treatment of magnetization that is transferred during the INEPT steps of the HSQC (the detected magnetization), as well as the reservoir magnetization from local and remote protons that are typically stored along z. The superscript $^{(r)}$ is used in the following to indicate such *remote* protons.

All parameters depend critically on the overall spin system and can therefore tremendously vary within a sample. The size of a spin system indicated by its overall number of coupled protons n, as well as the number of protons k bound directly to ^{13}C, i.e. $k = 2$ for a CH_2 group, are especially important.

The polarization of each of the k protons bound directly to ^{13}C is described by $M_z(0)$ before the excitation. The resulting remaining polarization after the ASAP-HSQC experiment is

$$M_z(\tau_{seq}) = M_z(0)\cos(\beta)\cdot E_{seq} \tag{14}$$

which recovers to

$$M_z(\tau_{seq} + \tau_{rec}) = M_z(\tau_{seq})E_1 + M_0(1 - E_1) \tag{15}$$

due to T_1 relaxation.

In addition, $(n - k)$ spins need to be considered that are part of the spin system consisting of altogether n protons that are not covalently bound to ^{13}C. For these remote spins the corresponding equations for the reservoir polarization $M_z^{(r)}$ are

$$M_z^{(r)}(\tau_{seq}) = M_z^{(r)}(0)E_{seq}^{(r)}, \tag{16}$$

$$M_z^{(r)}(\tau_{seq} + \tau_{rec}) = M_z^{(r)}(\tau_{seq})E_1^{(r)} + M_0^{(r)}\left(1 - E_1^{(r)}\right), \tag{17}$$

with the equilibrium reservoir magnetization $M_0^{(r)}$ and the corresponding loss constant $E_{seq}^{(r)}$ during the HSQC and T_1 recovery according to $E_1^{(r)} = \exp\left(-\tau_{rec}/T_1^{(r)}\right)$.

In the last remaining step of the ASAP-HSQC, the isotropic mixing period of duration τ_{mix}, ^{13}C-bound and reservoir proton polarization are mixed. In an ideal mixing situation, polarization is equally distributed among all n protons of the spin system. At the time $T_R = \tau_{seq} + \tau_{rec} + \tau_{mix}$, all spins, local and remote, have the polarization

$$\begin{aligned} M_z(T_R) = M_z^{(r)}(T_R) = E_{mix}\cdot M_z(\tau_{seq} + \tau_{rec})\tfrac{k}{n} \\ + E_{mix}^{(r)}\cdot M_z^{(r)}(\tau_{seq} + \tau_{rec})\tfrac{n-k}{n}, \end{aligned} \tag{18}$$

assuming that all proton spins are affected by slight losses during the TOCSY period according to the empirically derived factors E_{mix} and $E_{mix}^{(r)}$. Steady state conditions are again ensured by

$$M_z(T_R) = M_z(0), \tag{4}$$

The derived relations form systems of equations that can be rearranged in matrices. The pulse sequence affects the polarization according to

$$\overrightarrow{M_z}(\tau_{seq}) = \underbrace{\begin{pmatrix} M_z(\tau_{seq}) \\ M_z^{(r)}(\tau_{seq}) \end{pmatrix}}_{\overrightarrow{M_z}(\tau_{seq})} = \underbrace{\begin{pmatrix} \cos\beta\cdot E_{seq} & 0 \\ 0 & E_{seq}^{(r)} \end{pmatrix}}_{\mathbf{P}} \underbrace{\begin{pmatrix} M_z(0) \\ M_z^{(r)}(0) \end{pmatrix}}_{\overrightarrow{M_z}(0)}, \tag{19}$$

while the subsequent recovery is described by

$$\overrightarrow{M_z}(\tau_{seq} + \tau_{rec}) = \underbrace{\begin{pmatrix} E_1 & 0 \\ 0 & E_1^{(r)} \end{pmatrix}}_{\mathbf{R}} \overrightarrow{M_z}(\tau_{seq}) + (\mathbb{1} - \mathbf{R}) \underbrace{\begin{pmatrix} M_0 \\ M_0^{(r)} \end{pmatrix}}_{\overrightarrow{M_0}} \tag{20}$$

and the idealized ASAP mixing period by

$$\overrightarrow{M_z}(T_R) = \overrightarrow{M_z}(0) = \underbrace{\frac{1}{n}\begin{pmatrix} kE_{mix} & (n-k)E_{mix} \\ kE_{mix}^{(r)} & (n-k)E_{mix}^{(r)} \end{pmatrix}}_{\mathbf{T}} \overrightarrow{M_z}(\tau_{seq}+\tau_{rec}). \quad (21)$$

For the steady state condition the matrix equation

$$\overrightarrow{M_z}(0) = \mathbf{T}\left(\mathbf{RP}\cdot\overrightarrow{M_z}(0) + (\mathbb{1}-\mathbf{R})\overrightarrow{M_0}\right), \quad (22)$$

has to be solved. The equation can be rearranged to

$$\overrightarrow{M_z}(0) = (1-\mathbf{TRP})^{-1}\cdot\mathbf{T}(\mathbb{1}-\mathbf{R})\overrightarrow{M_0}, \quad (23)$$

which is then solved to obtain the steady state polarization at time 0, right before the next excitation element,

$$M_z^{ASAP}(0) = \frac{E_{mix}\cdot\left(kM_0(1-E_1)+(n-k)M_0^{(r)}\left(1-E_1^{(r)}\right)\right)}{n-(n-k)E_{mix}^{(r)}E_{seq}^{(r)}E_1^{(r)} - kE_{mix}E_{seq}E_1\cos(\beta)}, \quad (24)$$

and the resulting signal intensity after excitation,

$$M_x^{ASAP}(\tau_{seq}) = E_{seq}^{*}\sin(\beta) \cdot \frac{E_{mix}\left(kM_0(1-E_1)+(n-k)M_0^{(r)}\left(1-E_1^{(r)}\right)\right)}{n-(n-k)E_{mix}^{(r)}E_{seq}^{(r)}E_1^{(r)} - kE_{mix}E_{seq}E_1\cos(\beta)}. \quad (25)$$

The steady state polarization of the ASAP-HSQC depends on the excitation angle but is greatly affected by the contribution of remote reservoir polarization. The coupling and mixing of k local spins and $n-k$ remote spins changes the optimal angle to

$$\cos(\beta_{opt}^{ASAP}) = \frac{kE_{seq}E_{mix}E_1}{n-(n-k)E_{seq}^{(r)}E_{mix}^{(r)}E_1^{(r)}}. \quad (26)$$

In most cases $\cos(\beta_{opt}^{ASAP})$ is larger than the optimal angle $\cos\beta_{opt}^{ALSO}$ in the ALSOFAST-HSQC. Assuming perfect HSQC and mixing efficiency by $E_{mix} = E_{mix}^{(r)} = E_{seq} = E_{seq}^{(r)} = E_{seq}^{*} = 1$ and no remote spins by $n = k$, Eq. (26) is identical to Eq. (7), the original Ernst angle definition.

2.5. Progressive excitation

For short experiments, when a steady state is not reached, a different solution with individually optimized flip angles can be advantageous. For each scan, different flip angles can be adjusted to achieve constant and maximum signal intensities. The condition of constant signal intensity from each scan is particularly important for 2D experiments. We first introduce the previously derived progressive excitation for a one-pulse experiment [36–38] before developing numerical solutions for progressively excited HSQC experiments.

The index i is used to indicate individual scans out of an experiment with N scans. Starting with the polarization $M_{z,i}(0)$ at the beginning of scan i, a pulse with flip angle β_i and negligible duration will create the magnetization

$$M_{z,i}(0_+) = M_{z,i}(0)\cdot\cos(\beta_i) \quad \text{and} \quad (27)$$

$$M_{x,i} = M_{z,i}(0)\cdot\sin(\beta_i)\cdot E_{seq}^{*}. \quad (28)$$

Depending on the experiment, the polarization then evolves for the repetition time T_R until the end of the scan and the beginning of the next scan, where

$$M_{z,i+1}(0) = M_{z,i}(T_R). \quad (29)$$

In contrast to the steady state model of the Ernst angle excitation (see Eq. (4)), we now require constant signal intensity

$$M_{x,i+1} = M_{x,i} \quad (30)$$

provided by

$$M_{z,i}(0)\sin(\beta_i) = M_{z,i+1}(0)\sin(\beta_{i+1}). \quad (31)$$

For maximum SNR, combined with the condition that all magnetization is used by the last scan, i.e.

$$\beta_N = \frac{\pi}{2} = 90^\circ, \quad (32)$$

the final element N of the sequence is fixed.

If infinitely slow T_1 relaxation is assumed, the polarization is not changing after the pulse and

$$M_{z,i}(0_+) = M_{z,i}(T_R) = M_{z,i+1}(0). \quad (33)$$

Using Eqs. (27) and (33) to replace $M_{z,i+1}(0)$ on the right hand side of Eq. (31) leads to

$$M_{z,i}(0)\sin(\beta_i) = M_{z,i}(0)\cos(\beta_i)\sin(\beta_{i+1}). \quad (34)$$

Trigonometric substitution and decrementing all indices by 1 yields the recursive solution

$$\beta_{i-1} = \arctan(\sin(\beta_i)) \quad (35)$$

that allows calculating all β_i starting with the final $\beta_N = 90^\circ$ element.

In the presence of T_1 relaxation, polarization behaviour is described by

$$M_{z,i+1}(0) = M_0 + \left(M_{z,i}(0_+) - M_0\right)\cdot E_1. \quad (36)$$

Using Eq. (36) to replace $M_{z,i+1}$ on the right hand side of Eq. (31) and decrementing all indices by 1 leads to the equation

$$M_{z,i-1}(0)\sin(\beta_{i-1}) = \left(M_0 + \left(M_{z,i-1}(0)\cos(\beta_{i-1}) - M_0E_1\right)\right)\sin(\beta_i) \quad (37)$$

that has to be solved to obtain a recursive solution. Unfortunately, due to the occurrence of $M_{z,i-1}(0)$ in the equation, boundary conditions for the first and the last scan exist. A numerical solution can be found iteratively by guessing an initial set of $M_{z,i}$, then solving for all β_i, and improving the guess for $M_{z,i}$ using β_i. This is repeated until sufficiently high and constant signal intensities are reached.

2.5.1. Progressive excitation for ALSOFAST experiments

To apply the considerations with respect to the ALSOFAST-HSQC from the previous section to the progressive excitation scheme, Eqs. (27) and (28) are modified to

$$M_{z,i}(0_+) = E_{seq}\cdot M_{z,i}(0)\cdot\cos(\beta_i) \quad \text{and} \quad (38)$$

$$M_{x,i} = E_{seq}^{*}\cdot M_{z,i}(0)\cdot\sin(\beta_i)\cdot E_{seq}^{*}. \quad (39)$$

The result of Eq. (37) is changed to

$$M_{z,i-1}(0)\sin(\beta_{i-1}) = \left(M_0 + \left(M_{z,i-1}(0)\cos(\beta_{i-1})E_{seq} - M_0\right)E_1\right)\sin(\beta_i). \quad (40)$$

The occurrence of $M_{z,i-1}(0)$ in the equation, again requires iterative numerical solving.

2.5.2. Progressive excitation for ASAP experiments

For ASAP-type experiments, the averaging of proton polarization by the mixing sequence before excitation has to be included and equations get more complex. After excitation, magnetization for the ALSOFAST and ASAP approaches behave similar until the end of τ_{rec}

$$M_{z,i}(\tau_{seq}+\tau_{rec}) = M_0 + \left(M_{z,i}(0_+) - M_0\right)\cdot E_1. \quad (41)$$

In the ASAP experiment T_R is not yet reached and the mixing step follows. After this step, all protons have the polarization

$$M_{z,i}(T_R) = M_{z,i}^{(r)}(T_R) = \frac{k}{n} \cdot M_{z,i}(\tau_{seq} + \tau_{rec}) E_{mix} + \frac{n-k}{n} \cdot M_{z,i}^{(r)}(\tau_{seq} + \tau_{rec}) E_{mix}^{(r)}. \quad (42)$$

Expanding all the time points in this equation to the beginning of scan i or $i+1$ leads to the final equation for the ASAP experiment

$$\begin{aligned} M_{z,i}(0)\sin(\beta_i) = {} & \tfrac{k}{n} \cdot E_{mix} \cdot M_0 \cdot \sin(\beta_{i+1}) \\ & + \tfrac{k}{n} \cdot E_{seq} E_1 E_{mix} \cdot M_{z,i}(0) \cdot \cos(\beta_i) \sin(\beta_{i+1}) \\ & - \tfrac{k}{n} \cdot E_1 E_{mix} \cdot M_0 \cdot \sin(\beta_{i+1}) \\ & + \tfrac{n-k}{n} \cdot E_{mix}^{(r)} \cdot M_0^{(r)} \cdot \sin(\beta_{i+1}) \\ & + \tfrac{n-k}{n} \cdot E_{seq}^{(r)} E_1^{(r)} E_{mix}^{(r)} \cdot M_{z,i}^{(r)}(0) \cdot \sin(\beta_{i+1}) \\ & - \tfrac{n-k}{n} \cdot E_1^{(r)} E_{mix}^{(r)} \cdot M_0^{(r)} \cdot \sin(\beta_{i+1}) \\ = {} & \sin(\beta_{i+1}) \cdot \\ & \left[E_{mix} \tfrac{k}{n} \left(M_0 + E_1 \left(M_{z,i}(0) \cos(\beta_i) E_{seq} - M_0 \right) \right) \right. \\ & \left. + E_{mix}^{(r)} \tfrac{n-k}{n} \left(M_0^{(r)} + E_1^{(r)} \left(M_{z,i}^{(r)}(0) E_{seq}^{(r)} - M_0^{(r)} \right) \right) \right]. \end{aligned} \quad (43)$$

Again, the progressing flip angles β_i can be numerically derived from this equation.

3. Comparing conventional, ALSOFAST-, and ASAP-HSQC in the steady state

3.1. Magnetization development during a scan

The equations derived in the previous chapters allow the calculation of polarization over the course of a scan of the experiment.

The evolution of magnetization in such a scan after reaching the steady state is visualized in Fig. 4 using an example spin system and time settings that resemble a typical small molecule in a fast experiment: A CH group next to a CH_2 group is considered ($k = 1$ and $n = 3$); relaxation times were taken to be $T_1 = T_1^{(r)} = 1$ s; and losses due to the HSQC sequence and mixing periods were considered by $E_{seq} = E_{seq}^{(r)} = 0.9$ and $E_{mix} = E_{mix}^{(r)} = 0.98$ (estimated from the steady state experiments described later); finally, $T_R = 0.2$ s was chosen. When following the time development, the initial polarization is converted into measurable coherence according to $\sin(\beta)$. Some of the coherence is lost according to $E_{seq}^{(r)}$ during the pulse sequence while the larger part contributes to the FID that is acquired during τ_{rec}. Also a part of the remaining polarization is lost during the pulse sequence according to E_{seq}. During τ_{rec}, the polarization recovers partially due to T_1 relaxation. The repetition time $T_R = 0.2$ s is below $T_1 = 1$ s, allowing only incomplete relaxation between scans.

In the conventional HSQC, only low initial polarization is present, which is then completely exhausted by the pulse sequence. Consequently, the conventional experiment has very low steady state polarization and the lowest signal intensity for the given conditions (Fig. 4A).

Using the optimized β pulse ($\beta_{opt}^{ALSO} = 42°$) in the ALSOFAST case, polarization can be preserved from previous scans and contributes to the steady state polarization. The higher polarization overcompensates the lower flip angle and the steady state signal intensity is increased compared to the conventional HSQC (Fig. 4B).

The ASAP-HSQC sequence results in a larger optimal flip angle $\beta_{opt}^{ASAP} = 60°$. Protons that are not directly bound to ^{13}C contribute to remote polarization. As the β-type excitation in reality is achieved by an INEPT transfer element with shortened transfer delays, this remote polarization is not converted to coherence by the β excitation. Over the course of the scan, it is therefore always higher than the active polarization, until all proton magnetization is averaged in the mixing step of the ASAP-HSQC. The higher available overall polarization is the reason for the increased optimal excitation angle, and the ASAP-HSQC yields highest signal intensity (Fig. 4C).

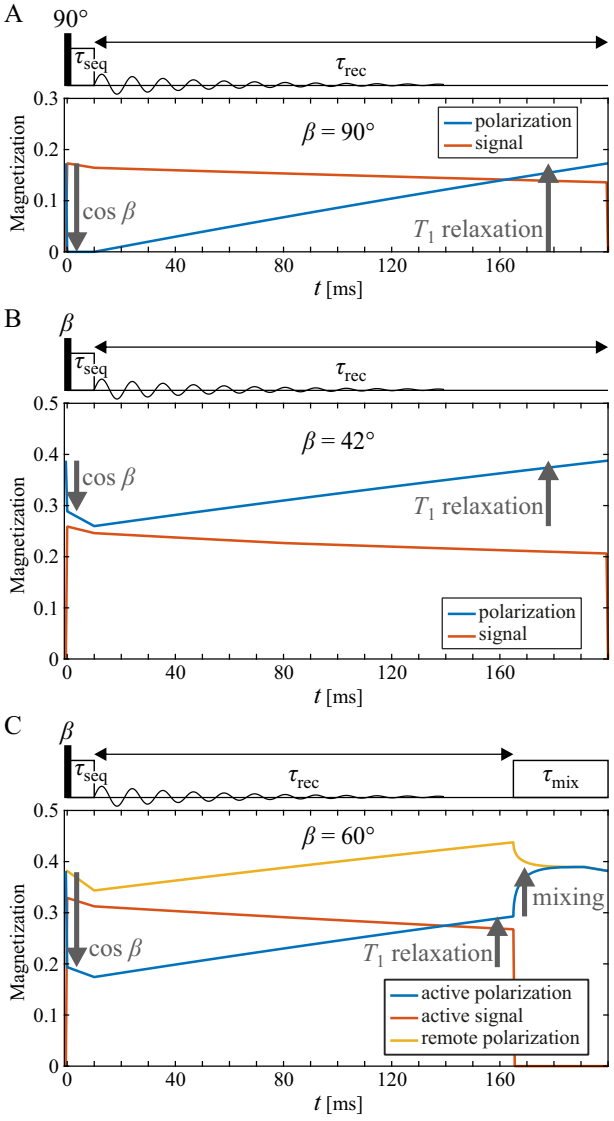

Fig. 4. Steady-state polarization (blue) and signal (red) over the course of a single scan with optimal excitation angle β_{opt}. The major events, changes of overall active polarization, are labeled by gray arrows: excitation with a certain flip angle, exponential T_1 relaxation, and polarization sharing by a mixing sequence (where applicable). Relaxation and experiment imperfection losses (E_{seq} and E_{mix}) are not labeled but included and indicated as linear decays. (A) Conventional HSQC featuring full excitation: polarization is lowered to 0 by each scan. (B) ALSOFAST-HSQC: Ernst angle excitation with optimal $\beta = 42°$ partially conserves the polarization reservoir. (C) ASAP-HSQC: Optimal $\beta = 60°$ is higher than for the ALSOFAST-HSQC. Polarization sharing between one active and two remote spins is included – the polarization of remote spins is also shown (yellow). The duration of the mixing sequence results in a reduced relaxation delay τ_{rec}. (Simulation details are given in Section 3.1 in the main text. For interpretation of the references to color in this figure legend, the reader is referred to the web version of this article.)

3.2. Theoretical comparison

From the descriptions derived in the previous section, the steady state of the different experiments can be compared. As shown in Eq. (11), the ALSOFAST-HSQC increases the steady state polarization when interscan relaxation is incomplete due to the retained polarization reservoir. Fig. 5A shows the polarization that

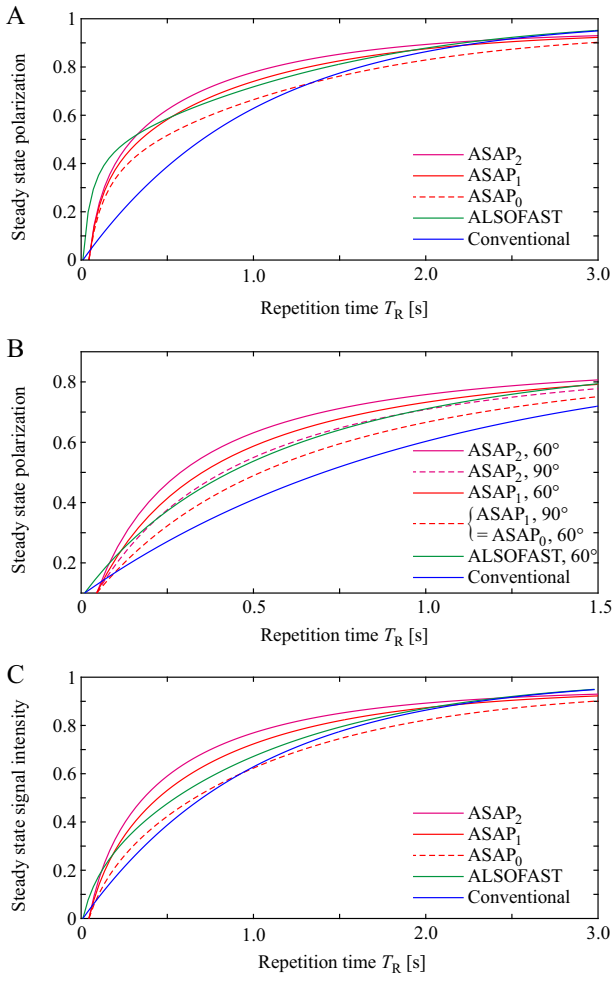

Fig. 5. Comparison of theoretical steady state polarization and signal intensities for the conventional HSQC (blue), ALSOFAST-HSQC (green), and ASAP-HSQC with different numbers of remote/passive spins indicated by subscript (red: no reservoir or 1 remote spin; magenta: 2 remote spins). $T_1 = 1$ s relaxation time, 10 ms pulse sequence duration, and 35 ms mixing time is assumed. (A) Steady state polarization at the beginning of each scan with optimal Ernst angle type excitation. (B) Steady state polarization at the beginning of each scan with fixed excitation. Contribution of remote spins in the ASAP experiment compensates higher excitation at equal polarization resulting in higher signal intensities. (please note the different axis ranges) (C) Steady state signal intensities with optimal Ernst angle type excitation resulting from the polarization shown in A. (For interpretation of the references to color in this figure legend, the reader is referred to the web version of this article.)

is available over a range of repetition times with the optimized Ernst angle equivalent. In the simulation $E_{seq} = E_{seq}^{(r)} = 0.95$, $E_{mix} = E_{mix}^{(r)} = 0.95$, and $T_1 = T_1^{(r)} = 1$ s was considered. In the ASAP case spin systems with $k = n = 1$ (ASAP$_0$), $k = 1, n = 2$ (ASAP$_1$), as well as $k = 1, n = 3$ (ASAP$_2$) corresponding to a single proton coupled to no, one, or two further protons, respectively, was chosen to resemble the effect of ideal mixing. During fast repetition, the ALSOFAST-HSQC (green) provides significantly higher polarization compared to the conventional experiment (blue) while polarizations converge with longer relaxation delays. Compared to the ALSOFAST-HSQC, including a mixing sequence without remote protons (ASAP$_0$, dashed red) leads to reduced polarization over the whole range of repetition times.

The difference between ALSOFAST and ASAP$_0$ is caused by three effects. Usually, the isotropic mixing time is 34.5 ms long, lowering the period of recovery τ_{rec} by the same amount for any given repetition time T_R. In Fig. 5 and similar plots, this results in the shift towards higher T_R of all ASAP curves. Furthermore, even in the absence of remote spins, the isotropic mixing lowers the available magnetization by roughly 5%, compared to the ALSOFAST experiment. As a third, smaller, effect, the Ernst angle is slightly lower due to the decrease of magnetization and reduced delay. A plot of the Ernst angles used is shown in the Supporting Information.

In contrast, the presence of remote protons (ASAP$_1$ and ASAP$_2$, solid red and magenta, respectively) compensates these losses and can lead to highest polarizations.

Looking at the influence of remote protons in more detail, Fig. 5B shows the polarization at fixed transfer delays corresponding to effective flip angles. Going from the ALSOFAST (green) to the ASAP experiment without remote protons (ASAP$_0$, dashed red) while keeping the excitation angle constant, leads to polarization similar to the ALSOFAST-HSQC, however, with reduced magnitude from mixing sequence losses (E_{mix}) and with increased pulse sequence duration due to the mixing time. Essentially, the ASAP$_0$ polarization is scaled down and shifted to longer repetition times compared to the ALSOFAST polarization. Including a single remote spin in the calculation, both effects are compensated (ASAP$_1$, solid red). A second remote spin increases polarization further (solid magenta), or allows increasing the excitation angle to 90° (dashed magenta) without loss of polarization compared to the ALSOFAST experiment (green).

It is interesting to compare the polarization of the 60° excitation ASAP$_0$ without remote spins and the 90° excitation ASAP$_1$ with a single remote spins. Eq. (24) shows both cases have mathematically equal polarization, the reservoir of non-excited magnetization in the 60° case is replaced by the reservoir consisting of a single remote spin. In both cases 50% of the magnetization is preserved, but the increased excitation angle yields 15% higher signal intensity. Similar equalities can be found for other atom counts and excitation angles, however, at non-integer values.

Knowledge of the polarization allows calculation of the steady state signal intensity per scan as shown in Fig. 5C for the different experiments at optimized excitation angle. In principal, the conventional HSQC is a special case of the ALSOFAST experiment with $\beta = 90°$. The very definition of the Ernst angle – the flip angle yielding maximum steady state signal intensity – ensures a signal increase for the ALSOFAST-HSQC over the conventional experiment. Therefore, the ALSOFAST experiment always provides higher or equal intensity compared to the conventional experiment.

Looking at the achievable SNR per single scan, several comparisons are possible. The arrows in Fig. 6 indicate differences between conventional and fast experiments for several cases, taking the conventional experiment with a repetition time of 1 s as reference: Constant repetition time T_R, i.e. constant overall experiment duration, provides an increase in single-scan SNR of 7% to 22% (a). The lower limit of T_R is the acquisition time, which lies typically within 100 ms to 200 ms for a full bandwidth HSQC. Lowering T_R to 200 ms reduces the single-scan SNR to approximately 50% for the fast methods and 27% for the conventional HSQC (c). Reduction of T_R and the experiment duration by half as a compromise decreases the single-scan SNR of the conventional HSQC to 62% and 77–94% for the fast experiments (b). Horizontal comparison indicates possible time savings. At constant single-scan SNR, T_R and the overall duration can be reduced by 15–40% for the ALSOFAST and ASAP methods, respectively (d).

A common alternative to the conventional HSQC experiment is the sensitivity-improved HSQC (HSQC-SI), which can provide higher signal intensity and SNR [47,48]. It utilizes an expanded transfer element after t_1 evolution. This transfer element has to be adjusted for a certain multiplicity. It can be optimized for CH groups only, providing an enhancement factor of $\sqrt{2} \approx 1.41$, but no enhancement for CH_2 and CH_3 groups. Commonly, however, the transfer is optimized for CH_2 groups. The experiment then

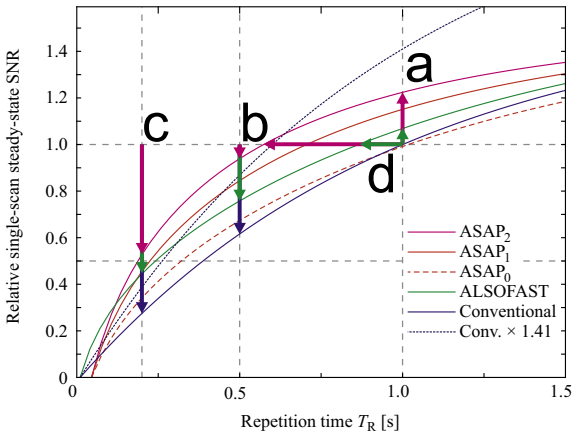

Fig. 6. Signal intensity per single scan and experiment duration comparison, normalized with respect to the conventional experiment at $T_R = T_1 = 1$ s; signal gain/loss for different repetition times and therefore overall durations as well as time savings can be derived. For ASAP and ALSOFAST, Ernst angle excitation is assumed; ASAP data is shown for 0 to 2 reservoir spins (ASAP$_0$ to ASAP$_2$); (*a*) SNR gain for ALSOFAST/ASAP-HSQC with unchanged experiment timing ($T_R = T_1 = 1$ s). (*b*) SNR loss for all three methods at half experiment duration ($T_R = 0.5 \cdot T_1$). (*c*) SNR loss for all three methods with rapid acquisition ($T_R = 200$ ms). (*d*) Time saving for ALSOFAST/ASAP-HSQC at equal SNR. Arrows are drawn for ALSOFAST-HSQC, ASAP-HSQC with two passive spins, and conventional HSQC. The ideal SNR of a CH group in the *sensitivity-improved* HSQC (HSQC-SI) with transfer optimized for CH is included by multiplying the conventional data by 1.41 [47,48].

provides an enhancement factor of $\sqrt{1+0.71^2} \approx 1.22$ for CH groups, $\sqrt{1+0.50^2} \approx 1.12$ for CH_2 groups, and $\sqrt{1+0.35^2} \approx 1.06$ for CH_3 groups (for more details please refer to the supporting information). The enhancement comes at the price of increased sequence duration, therefore increased magnetization loss due to relaxation, increased number of RF pulses, and, most importantly, the additional transfer step can introduce artifacts caused by proton-proton coupling or off-resonance effects [49,50]. The maximum intensity of an ideal sensitivity-improved HSQC is estimated by multiplying the conventional data by the respective factor.

Besides reducing the overall experiment duration, shorter repetition time at unchanged experiment duration i.e. more repetitions, can provide several advantages. It allows increased resolution in the indirectly detected dimension, i.e. increasing the maximum value of t_1, when T_2 relaxation time is sufficiently long. Instead of increasing the resolution, it is also possible to increase the spectral width of the spectrum. Finally, it provides the possibility for additional artifact suppression by pulse phase cycling. While the accurate simulation of artifact intensity requires a complete simulation of the spin system, which exceeds the frame of this work, in general, a higher count of repetitions provides additional opportunities for artifact suppression.

The connection between the number of repetitions and the SNR is more complicated. The relative available SNR of experiments of equal overall duration will now be compared. Fig. 7 shows the signal intensity of a single scan divided by the square root of the duration of a single scan. The length of the acquisition time is assumed to be fixed, e.g. limited by the allowed decoupling time, and no effects of T_2 relaxation are included. The conventional experiment achieves highest SNR at 1–1.5 s, while optimal values of T_R for the fast experiments are in the range of 200–500 ms.

Considering CH groups, in ideal cases and when the transfer is optimized for CH groups, a sensitivity-improved HSQC can exceed the SNR of the ASAP-HSQC. In the more common case of transfer optimized for CH_2 groups, the advantage disappears. For CH_2 and CH_3 groups, ASAP experiments suffer from the effectively low number of available remote spins, while in the HSQC-SI, only very small enhancement is achievable.

3.3. Experimental verification

In the next step, we compared the theoretical predictions with experimental data. For this purpose, we prepared a steady state similar to the steady state of an HSQC experiment in a specially devised NMR experiment. The polarization of this steady state is then transfered to proton coherence and measured. The pulse sequence of the sequence termed HSQC-recovery is shown in Fig. 8. It consists of a series of 1D-HSQC elements. The preparation block including an incremented recovery delay τ_{rec} is repeated 64 times and followed by a readout block. The preparation HSQC contains two INEPT steps, the transfer delay Δ' of the first was varied to achieve incomplete transfer in the CH_n spin system with an effective angle of $\beta = 2\pi \cdot {}^1J_{CH} \cdot \Delta'$. All non-transferred magnetization is returned to polarization as required for Ernst angle-equivalent excitation. The delay Δ of the first preparation INEPT step and both INEPT steps of the readout HSQC element was set to $\Delta = (4 \cdot 145\ \text{Hz})^{-1}$.

Parameters within the preparation sequence allow recreation of the conditions of conventional, ALSOFAST-, and ASAP-HSQC. The pulse phases φ_1 and φ_2 control dephasing or conservation of the reservoir magnetization, i.e. the difference between conventional and ALSOFAST-HSQC. For ASAP-like conditions, a 34.5 ms DIPSI-2 mixing sequence was applied after the recovery delay and before the next HSQC element. The readout signal is proportional to the steady state polarization; integration and normalization with respect to a fully relaxed experiment ($\tau_{rec} = 10$ s, approximating M_0) yields the normalized steady state polarization M_z^{exp}.

The measured steady state polarization using the described sequences is shown in Fig. 9 for five different positions of menthol in $CDCl_3$. For each repetition time T_R, the optimal transfer delay, i.e. effective flip angle, to yield maximum intensity for the molecule as a whole – not optimal for all individual positions was chosen. As expected, the conventional HSQC polarization is always lower than the ALSOFAST polarization. The steady state SNR derived from the polarization is shown in Fig. 10. Again, the ALSOFAST-HSQC shows higher values than the conventional experiment. Please note that the signal gain is lower than the polarization gain as the excitation angle is usually lower than 90°.

T_1 times of menthol were not determined accurately, but are approximately 1.5 s for the ^{13}C-bound protons. The conventional polarization reflects the relaxation time and varies only little between the positions. The ASAP-HSQC polarization is similar to the ALSOFAST polarization for positions with common proton constellations (B, C). The measured values agree very well with the ASAP$_1$ and ASAP$_2$ cases of Fig. 5. For a low relative number of remote protons like in the methyl group 8 (E) it falls below ALSOFAST values, while it exceeds it for ideal groups with many remote protons like the isopropyl subunit 7 (D). The polarization of the axial proton 1 next to the OH group is in the intermediate range, in spite of the lower number of surrounding protons. Presumably, the connection to the axial-axial coupling network around the ring provides a large reservoir of magnetization.

The optimal transfer delay of the ASAP-HSQC in general is longer than the one of the ALSOFAST-HSQC. The steady state signal intensity shown in Fig. 10, consequently, is higher in all cases but the methyl group (E). Like the polarization, also the signal intensities closely follow the theoretical values.

4. Progressive excitation

With the description derived for the different experiments, also achievable SNR for the individual scans of a progressive excitation experiment can be calculated and the behavior compared to a constant-excitation experiment. Typical constant-excitation

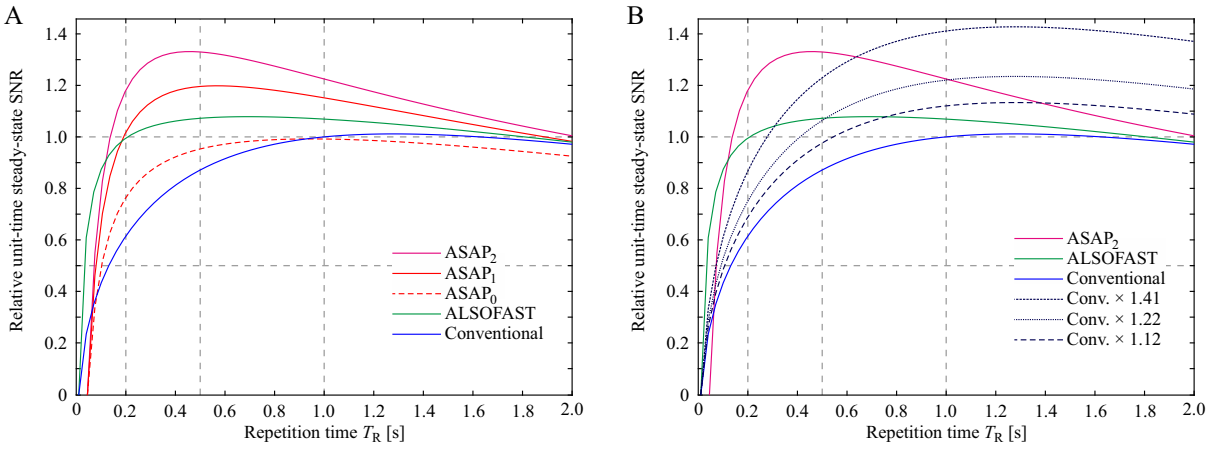

Fig. 7. Relative SNR per unit time achievable with different methods and different spin systems calculated by signal intensity per single scan divided by square root of the duration of a single scan. For ASAP and ALSOFAST, Ernst angle excitation is assumed; ASAP data is shown for 0 to 2 reservoir spins (ASAP$_0$ to ASAP$_2$) (A); The ideal SNR in the *sensitivity-improved* HSQC is included by multiplying the conventional data by a factor (B) [47,48]. Maximum enhancement is 1.41 for a CH group with transfer optimized for CH group. When transfer is optimized for CH_2 groups, enhancement is 1.22 and 1.12 for CH and CH_2 groups, respectively.

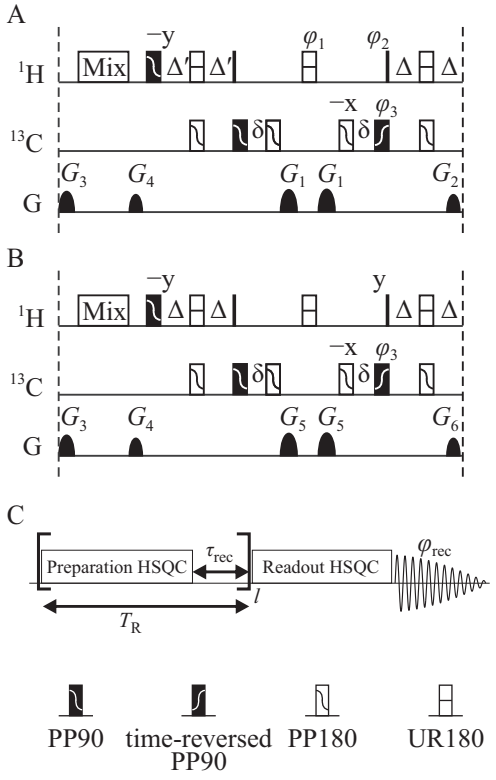

Fig. 8. Pulse sequence used for the HSQC recovery experiments. The sequence consists of two sub-sequences (A) a preparation HSQC and (B) a readout HSQC. (C) In the experimental setup the preparatory HSQC is followed by a delay, τ_{rec}, and then is run 1, 8, 16, or 64 times by changing the loopcounter l to show the difference between a scan run from thermal equilibrium and a scan in steady state. All pulses are x pulses, unless specified otherwise. φ_1 = x; φ_2 = y; φ_3 = x, −x; Switching the phase φ_1 from x to y, changes the reservoir alignment from z to $-z$. Switching the phase φ_2 from y to x, dephases the reservoir magnetization in the transversal plane. The fist INEPT delay Δ' can be adjusted to implement incomplete transfer and allow Ernst angle excitation. Solid black shapes represent 90° excitation pulses (PP90), unfilled shapes represent 180° refocussing (UR180) or inversion pulses (PP180) [33]. For evaluation, Δ' with maximum overall molecule intensity was used.

results are shown in Fig. 11 (filled squares, ■). Using the same setup for calculations as for Fig. 5, the corresponding sets of Ernst angles were calculated and used for excitation. The curves of polarization and signal intensity are proportional and, initially, both are very high, but decrease with the first scans. These initial scans are usually run as so-called dummy scans and their data is discarded or not recorded in steady-state experiments. After about 10 scans, the signal intensity stabilizes and steady-state data is generated.

Individual N flip angles for an experiment can be optimized using Eqs. (37), (40), and (43). The flip angles, polarization, and signal intensities of two such experiments are shown in Fig. 11 (filled circles, •). In comparison to the Ernst angle experiment, several features are visible. As expected, the flip angles start at values lower than corresponding Ernst angles and are increased with every scan. Polarization and signal intensity are no longer proportional as the increasing flip angle compensates the decreasing polarization. Dummy scans are not required to achieve constant signal intensities. The initial polarization, which is mostly discarded during the dummy scans in an experiment with constant excitation, increases the signal intensity of all scans during progressive excitation. Consequently, the achievable signal intensity is slightly higher after progressive excitation as compared to the steady state.

Including polarization sharing like in the ASAP-HSQC, the optimal flip angles are of course increased by the available remote reservoir polarization. To calculate the set of flip angles, however, the number of effective reservoir spins has to be known, and in most molecules only a compromise can be achieved. The theoretical results are shown in Fig. 11, ideal averaging by the mixing sequence is assumed. The averaging of active and remote polarization increases the available polarization and allows higher flip angles, especially in the later scans of the experiment.

For experimental verification, a 1D progressive excitation experiment optimized for T_1 relaxation was used by recording a pulse-acquire spectrum repeatedly in pseudo-2D fashion.

For this purpose, the standard Bruker pulse program for pseudo-2D acquisition was modified to use a list of pulse lengths and compared to a regular experiment where all the excitation angles were set to the corresponding Ernst angle. Menthol in $CDCl_3$ was used as a test sample. The signal intensities of the signal of the proton in 5-position (next to the methyl group) is plotted against the scan number in Fig. 12. As expected, the constant-flip angle excitation yields rapidly decaying signal intensities. The progressive-excitation method provides more constant intensity, and yields higher overall intensities. However, the relaxation properties of the system have apparently not been matched accurately, and signal intensity slowly rises over the course of the experiment. In the insert, the cumulative sum of intensity is shown for the two

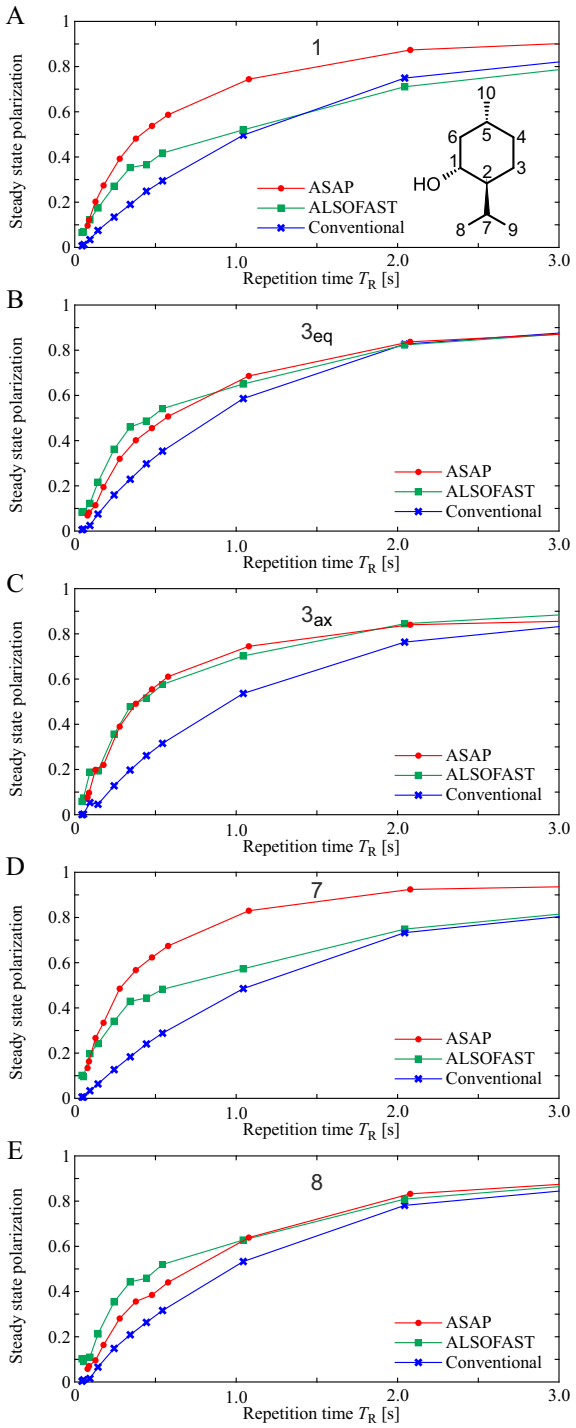

Fig. 9. Experimental comparison of steady state polarization M_z^{exp} between conventional HSQC, ALSOFAST- and ASAP-HSQC experiments for five different groups of menthol in $CDCl_3$. The proton at 1-position (A) has few neighboring protons but with high coupling constants. The equatorial 3_{eq} proton (B) has a large coupling to the 3_{ax} proton but only small coupling constants to the surrounding ring protons, while the axial proton (C) has large coupling constants to other axial protons as well. The two methyl groups provide a large reservoir for the proton at the 7-position (D). The methyl group at the 8-position (E), instead, has a small reservoir compared to the number of active protons.

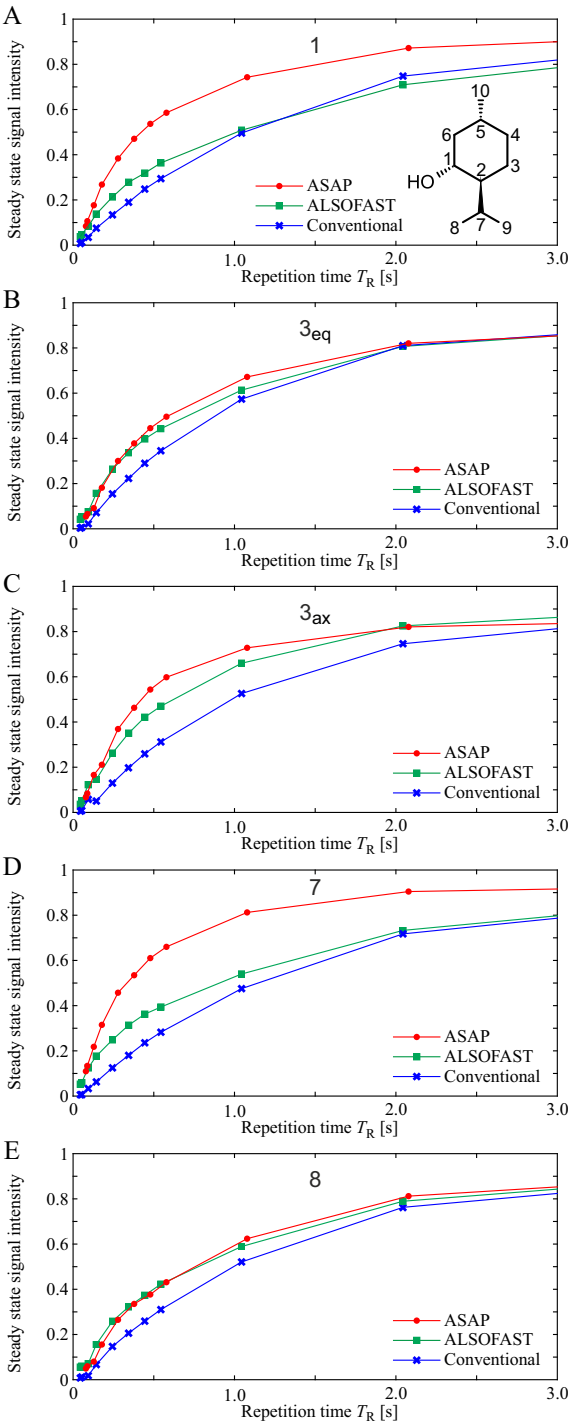

Fig. 10. Experimental comparison of steady-state SNR of a single scan M_x^{exp} between conventional HSQC, ALSOFAST- and ASAP-HSQC experiments for different groups of menthol in $CDCl_3$ (same groups as in Fig. 9).

experiments. Using progressive excitation, an approximately linear rise in intensity is achieved. Constant excitation yields higher intensity for the first scans while later scans contribute less and eventually, progressive excitation intensity exceeds constant excitation. In an experiment acquired with dummy scans, the first scans of constant excitation are discarded – and more intensity is lost.

The progressive excitation scheme was also implemented in an HMQC experiment to investigate the influence on lineshapes in the indirect dimension. A coherence order selecting echo/antiecho HMQC sequence was modified to include a list of variable pulse lengths for the ^1H excitation pulse and a purge gradient before the first pulse. The pulse sequence, implemented with minimal

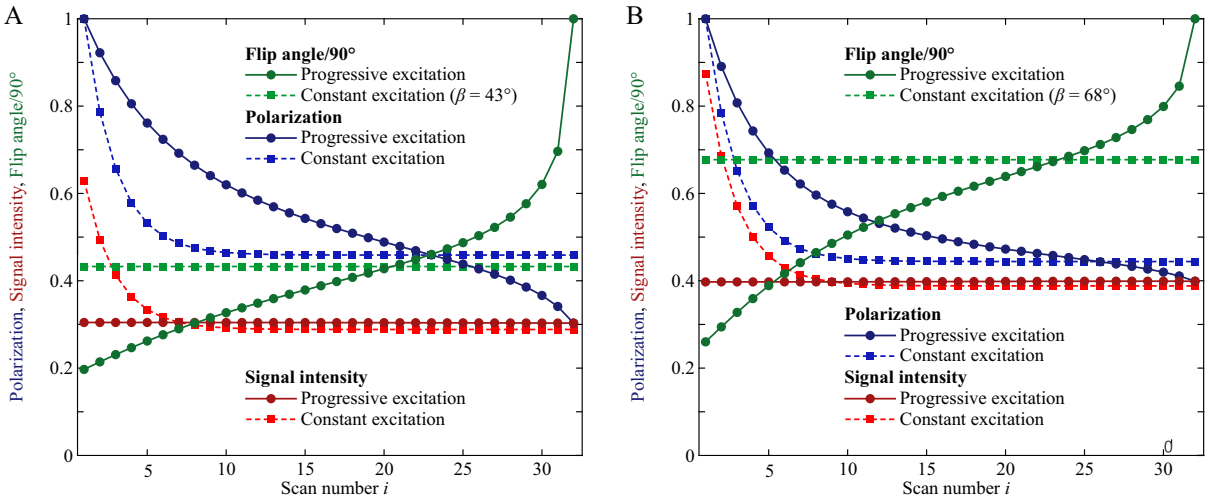

Fig. 11. Theoretical comparison of constant flip angle excitation with progressive excitation for constant signal intensity. For each scan flip angle, relative polarization, and signal intensity are shown. The constant excitation shows reaching a steady state after about 10 scans. To achieve constant signal intensity in a conventional setup (Ernst angle), the initial 8–16 scans would be discarded as dummy scans. In all cases, the progressive excitation signal intensity is only slightly above the steady state Ernst angle signal intensity. For the simulation, relaxation time $T_1 = 1$ s was assumed. Parameters were optimized for the recovery delay $\tau_{rec} = 200$ ms, and $N = 32$ scans. For magnetization losses, $E_{seq} = E_{seq}^{(r)} = 0.95$ and $E_{seq}^{*} = 1$ were used. (A) ALSOFAST method; optimized flip angles as described in Eq. (40); Ernst angle calculated by Eq. (13). (B) ASAP method for a $k = 1$ active spins in a spin system of $n = 3$. Optimized flip angles as described in Eq. (43); Ernst angle calculated by Eq. (26). $E_{mix} = E_{mix}^{(r)} = 0.95$.

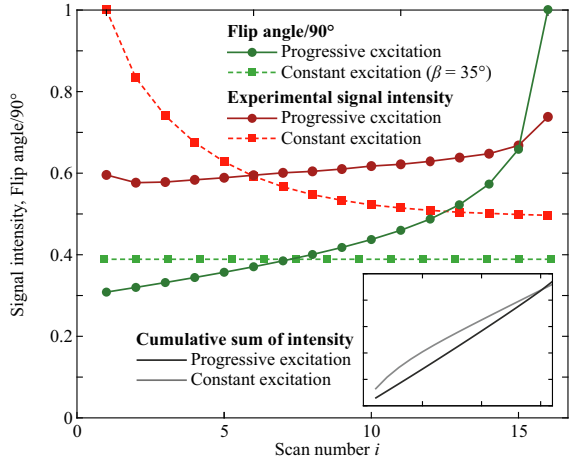

Fig. 12. Relative experimental SNR of the signal of H5-C5 of menthol in $CDCl_3$ and flip angles used in the experiment. $T_1 \approx 2.3$ s, $\tau_{rec} = 0.35$ s. 16 scans were recorded overall. $\tau_{rec} = 0.15 \cdot T_1$ was used for progressive excitation and $\beta = 35°$ was used for constant excitation. The insert shows the cumulative sum of intensities of the two experiments. Constant excitation initially has higher intensity, while progressive excitation yields a linear growth and eventually exceeds constant excitation. Final intensity ratio is 1 to 0.977 (progressive to constant excitation).

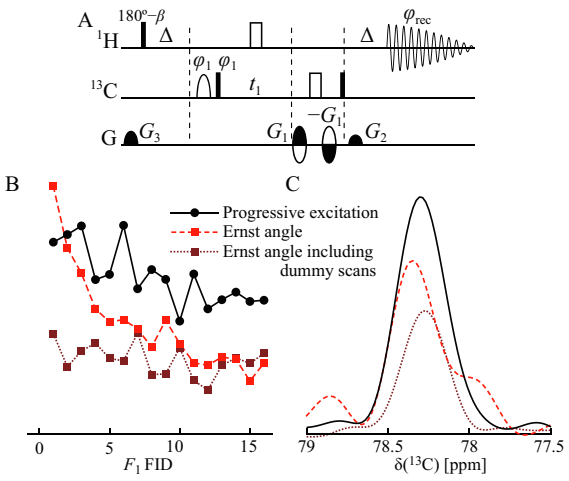

Fig. 13. Implementation of a progressive excitation β-excited HMQC experiment conducted on 1% $CHCl_3$ in Acetone-d_6. (A) HMQC pulse sequence with variable flip angle excitation. Except for the β pulse, filled rectangles represent 90° pulses, open rectangles 180° pulses. The first pulse on ^{13}C is an adiabatic chirped inversion pulse. Initially, all pulse phases in the sequence are x pulses, φ_1 and φ_{rec} are used for TPPI progression. Phase sensitivity in the indirect dimension is achieved via echo/antiecho coherence pathway selection using the gradients $G_1 = \pm 80\%$ and $G_2 = 40.2\%$. (B) Magnitude of $CHCl_3$ signal intensity for the complex points acquired in the experiment. Constant excitation is shown without (red dashed lines) and with 16 dummy scans (dark red dotted lines) next to optimized progressive excitation (black solid lines). T_1 for $CHCl_3$ was estimated to be above 60 s and the recovery delay was set to $\tau_{rec} = 0.15$ s. Optimal constant excitation was achieved with $\beta = 1.6°$. 1536×32 real points were acquired in 5 s without or 8 s with 16 dummy scans. (C) F_2 traces of the chloroform signal after Fourier transform to 4096×512 points.

pulses, is shown in Fig. 13A. The 180° pulse has to be accounted for when adjusting β by using $180° - \beta_i$ as flip angle.

In Fig. 13B, the corresponding comparison between a progressive excitation HMQC and a constant flip angle HMQC are illustrated. The spectra were acquired on the Bruker lineshape sample, 1% $CHCl_3$ (73 mmol/L) in acetone-d_6. T_1 of the molecule is > 60 s, best constant excitation results were achieved with $\beta = 1.6°$. The low flip angle and the low natural abundance of ^{13}C decrease the SNR of the sample to slightly above the single-scan detection limit on a 600 MHz spectrometer equipped with a cryogenically cooled triple resonance probehead.

The HMQC spectrum was acquired in regular echo/anti-echo mode, acquiring two complex FIDs in sequence per value of t_1. The absolute value of the FID was obtained by calculating the absolute value of the hypercomplex spectrum, i.e., after Fourier transform in the directly detected dimension, the absolute value of the echo spectrum and the anti-echo spectrum at resonance were added geometrically (root of sum of squares). In comparison, progressive excitation achieves highest signal and relatively constant signal intensities. While providing only slightly lower intensity, the constant flip angle experiment shows rapid signal intensity decline when run without dummy scans. This can cause line broadening and may also introduce phase errors when combining echo

and antiecho FIDs for phase-sensitivity in the indirect dimension. Performing dummy scans before the acquisition sacrifices a large fraction of the initial polarization, but provides constant signal intensity. The F_2 traces of the same spectra are shown in Fig. 13C. All spectra have very low SNR, originating from the short experiment duration. Comparing the three peaks, progressive excitation yields not only higher intensity, but also reduced line width and improved line shape.

5. Conclusion

5.1. Progressive excitation

Next to the steady state model and the adapted Ernst angle, a method for variable flip angle excitation in short experiments is presented. This idea was previously described, but to our knowledge never applied to multidimensional NMR spectroscopy [35–38]. Just like Ernst angle calculation, its application requires knowledge of the T_1 time, and additionally, a list of excitation pulses β_i has to be calculated, which is easily done in MATLAB or similar programs (see supporting information).

Mismatched parameters can cause deviating signal intensity, however, resulting in line shape distortions similar to experiments without dummy scans. Small flip angles are less prone to offset effects. The HMQC example, however, utilizes flip angles close to 180° which are very sensitive to detuning. For a more robust experiment, broadband pulse shapes with a range of flip angles are required, for which some solutions exist [51–54].

The concept could be demonstrated on a slowly relaxing sample, where only a small increase in SNR and improved lineshape could be achieved. Hyperpolarized samples can profit from similar treatment [37], and a larger gain is to be expected. Here, progressive excitation 2D NMR could be an alternative to ultrafast experiments [11,15].

A feature of variable excitation not addressed in this work is the possibility to intentionally create varying signal intensity. According to processing, lower signal intensity could be created for steps that are scaled down by the window function, to save polarization for FIDs with higher contribution. It should also be possible to use variable excitation to replace the dummy scans of a constant excitation experiment, to reach the steady state after a shorter number of scans.

5.2. Experiment comparison

Comparing the conventional and fast experiments, we could show, that the polarization and therefore SNR of the conventional and the ALSOFAST-HSQC are mostly determined by the spins' T_1 times and not highly dependent on the number of coupled spins the experiment is applied on. The ALSOFAST-HSQC clearly provides higher SNR than corresponding conventional HSQC experiments without sensitivity improvement. For short repetition times T_R even HSQC-SI sequences cannot reach the performance of ALSOFAST-type acquisition and most ASAP cases. Choice of ASAP- over ALSOFAST-HSQC, strongly depends on the molecule, i.e. the spin system in question. Considering relaxation properties, small molecules with long T_1 and T_2 times are ideal candidates for the ASAP-HSQC, larger molecules are more prone to saturation during the mixing sequence and can even have improved relaxation after selective excitation, so the ALSOFAST-HSQC is appropriate.

For samples providing abundant SNR in a conventional HSQC setup, simply reducing the polarization recovery time (τ_{rec}) incurs prohibitive losses in SNR and spectral quality. The ALSOFAST- and ASAP-HSQC provide a simple way to reduce measurement time significantly without similar losses. While the fast methods cannot always compensate the loss of SNR from each individual scan, they provide highest SNR per time, especially for reduced recovery times.

Instead of reducing the overall measurement time, the reduced recovery delay allows also for increased resolution in the indirectly detected dimension. As was shown before, especially with NUS, absurdly high resolution can be achieved in the time frame of a conventional experiment [33]. The simulations in this work, however, are more oriented towards experiments with conventional resolution and lack accuracy for longer experiments. As the neglected homonuclear couplings of reservoir protons will play an important role in experiments that approach resolution in the range of 10 Hz and below, models derived in this article will not be applicable. Increased spectral width or improved artifact suppression by pulse phase cycling is not limited by relaxation in the same way and can be applied whenever more than a single repetition per t_1 value is required.

For samples providing insufficient SNR in a conventional HSQC setup, i.e. samples that require a large number of accumulated transients to provide a complete spectrum, the fast methods can provide more SNR per overall time than the conventional HSQC. When optimized and applied to CH groups, the HSQC-SI SNR for longer τ_{rec} can be higher than the ASAP-HSQC SNR and may be preferred [47,48], usually, however, the HSQC-SI setup is optimized for CH_2 groups, where only small enhancement is possible. Interestingly, both experiments, the ASAP-HSQC and the HSQC-SI experiment, do not show large enhancements for CH_2 and CH_3 groups; in the ASAP-HSQC, the number of reservoir spins per active spin is halved and in the HSQC-SI, only incomplete transfer can be achieved. Unfortunately, a combination of an ASAP-like method with sensitivity-improved transfer has not yet been reported.

5.3. Steady state model

A novel mathematical model for the description of fast heteronuclear experiments like the ALSOFAST- and ASAP-HSQC is presented. It provides information on the polarization, optimal excitation angle, signal intensity, and SNR of a single scan from thermal equilibrium as well as the steady state of such experiments. Experimental data was acquired to verify the predictions of the model.

While some of the equations are quite complicated, at least for the ASAP Ernst angle, a rough estimate shall be given. Assuming a single active spin ($k = 1$) in a coupled system of n spins, parameter values $E_{seq} \approx E_{seq}^{(r)} \approx E_{mix} \approx E_{mix}^{(r)} \approx 0.95$ are realistic approximations for small molecules. The T_1 relaxation times of the molecules in question have to be estimated, but at least they will not vary greatly within a coupled system of spins, justifying $E_1 = E_1^{(r)}$. Fitting Eq. (26) to a more simple exponential equation yields

$$\cos(\beta_{opt}^{ASAP}) \approx (0.93 - 0.07n) \cdot \exp\left(-\frac{\tau_{rec}}{T_1 \cdot (0.8 - 0.07n)}\right). \quad (44)$$

This approximation is fairly accurate with less then 5° deviation over 2–4 spins and τ_{rec} of 0.01 to 1 T_1.

The model is not a complete quantum-mechanical simulation of the experiment, but contains coefficients $E_{seq} \leqslant 1$ to approximate magnetization losses due to relaxation within the pulse sequence, homo- and heteronuclear coupling, pulse imperfections, and other effects. Some of the effects are dependent on the sample and vary for the individual spins in a molecule, other effects are dependent on t_1 in a 2D experiment, and will change over the course of the 2D experiment. All of the effects are approximated by one value for ^{13}C-bound proton reservoir magnetization ($E_{seq}^{(r)}$), ^{13}C-bound proton detected magnetization (E_{seq}^{*}), and remote reservoir magnetization

($E_{seq}^{(r)}$). Considering a small molecule with similar and long relaxation times for all nuclear species involved, E_{seq} will not vary significantly for increment times much shorter than the relaxation times of carbon spins and the $1/J_{HH}$ coupling period. Equally, offset-dependent losses due to pulse imperfections are compensated by shaped broadband pulses and the coherence transfer depends on $\cos(\pi^1 J_{CH}\Delta)$, which at least within the aliphatic or the aromatic region will not vary extensively in conventional samples. The actual value $E_{seq} = 0.95$ used for most calculations was estimated from 1D-HSQC measurements, i.e. $t_1 \approx 0$. Deviation from experimental data is expected especially for experiments with high resolution in the indirectly detected dimension, i.e. high values of t_1, which was not examined in this work.

Comparison with experimental data reveals a shortcoming for the ASAP-HSQC model. The ideal mixing of spin polarization, i.e. averaging of all available spins, is useful to estimate the gain in signal intensity, however, is not accurate enough to allow quantification of the number of spins. In reality, magnetization transfer depends on homonuclear coupling constants which typically lie within the range of 4–15 Hz with 7 Hz being most common. Complete transfer in a two spin system is reached after $1/(2J) \approx 71$ ms for $J = 7$ Hz without considering saturation and relaxation. In the implementation, however, the optimal mixing time was usually found to be 34.5 ms and even in ideal cases only incomplete transfer can be achieved. In systems of more spins, the transfer function is more complicated, and unexpected effects like zero or negative transfer are possible [55–68]. Approximated calculation of simple transfer functions are a possible extension for the ASAP model.

The model also does not include the influence of surrounding polarization on a spin's T_1 relaxation. This is part of the Nuclear Overhauser Effect or Enhancement (NOE) and has been reported before [69–71]. For small molecules, the NOE contribution to the relaxation rate is negative, R_1^{NOE} depends on $-M_z^{(r)}$ (corresponding to a so-called *positive* NOE). The effect is small, we measured a maximum of 10% reduction in the R_1 rates, and decided not to include it in the model. For larger molecules, the NOE contribution to the relaxation rate is positive R_1^{NOE} depends on $+M_z^{(r)}$ (*negative* NOE), and the effect can become significant, leading generally to improved SNR in corresponding experiments. The BEST experiments and the SOFAST-HMQC exploit this effect [7,8,28,29]. To describe very large molecules and to embrace these experiments completely, NOE and polarization transfer by chemical exchange might have to be included in the model. However, in most large molecules, this will lead to increased SNR and corespondingly, experimental performance can exceed predictions by the model.

In summary, we derived four models for polarization and SNR for SOFAST/ALSOFAST- and ASAP-type experiments in the steady-state limit of long experiments and progressive excitation for very short experiments. Retaining reservoir polarization, the ALSOFAST experiment is always better than the conventional experiment. In most proton-rich spin systems, the ASAP experiment with an additional mixing step exceeds the ALSOFAST experiment. While the model represents only a rough estimate, for small to medium sized molecules it appears to predict experimental results quite well.

Competing interests

The authors have no competing interests to declare.

Acknowledgement

The authors thank the DFG [LU835/13-1] and the HFG programme BioInterfaces in Technology and Medicine for financial support. MRMK thanks Johanna Becker and David Schulze Sünninghausen for their help with the ALSOFAST/ASAP-HSQC sequences and David L. Goodwin for the math support.

Appendix A. Supplementary material

Supplementary data associated with this article can be found, in the online version, at https://doi.org/10.1016/j.jmr.2018.12.014.

References

[1] R.R. Ernst, W.A. Anderson, Application of Fourier transform spectroscopy to magnetic resonance, Rev. Sci. Instrum. 37 (1) (1966) 93–102, https://doi.org/10.1063/1.1719961.
[2] R.R. Ernst, Sensitivity enhancement in magnetic resonance, in: J.S. Waugh (Ed.), Advances in Magnetic Resonance, Advances in Magnetic and Optical Resonance, vol. 2, Academic Press, 1966, pp. 1–135, https://doi.org/10.1016/B978-1-4832-3115-0.50008-9, URL <https://www.sciencedirect.com/science/article/pii/B9781483231150500089> .
[3] R.R. Ernst, G. Bodenhausen, A. Wokaun, Principles of Nuclear Magnetic Resonance in One and Two Dimensions, International series of monographs on chemistry, Clarendon Press, 1990.
[4] A. Haase, J. Frahm, D. Matthaei, W. Hanicke, K.-D. Merboldt, FLASH imaging. Rapid NMR imaging using low flip-angle pulses, J. Magn. Reson. (1969) 67 (2) (1986) 258–266, https://doi.org/10.1016/0022-2364(86)90433-6, URL <https://www.sciencedirect.com/science/article/pii/0022236486904336> .
[5] J.D. Frahm, A.D. Haase, D.D. Matthaei, W. Haenicke, K.D.D. Merboldt, Method and device for rapid acquisition of spin resonance data for a space-resolved examination of an object, dE Patent App. DE19,853,504,734, Aug. 1986. URL <https://worldwide.espacenet.com/publicationDetails/biblio?CC=DE&NR=3504734>.
[6] S. Zhang, M. Uecker, D. Voit, K.-D. Merboldt, J. Frahm, Real-time cardiovascular magnetic resonance at high temporal resolution: radial FLASH with nonlinear inverse reconstruction, J. Cardiovasc. Magn. Reson. 12 (1) (2010) 39, https://doi.org/10.1186/1532-429X-12-39.
[7] P. Schanda, B. Brutscher, Very fast two-dimensional NMR spectroscopy for real-time investigation of dynamic events in proteins on the time scale of seconds, J. Am. Chem. Soc. 127 (22) (2005) 8014–8015, https://doi.org/10.1021/ja051306e, pMID: 15926816.
[8] P. Schanda, Ē. Kupče, B. Brutscher, SOFAST-HMQC experiments for recording two-dimensional heteronuclear correlation spectra of proteins within a few seconds, J. Biomol. NMR 33 (4) (2005) 199–211, https://doi.org/10.1007/s10858-005-4425-x.
[9] L. Mueller, Alternate HMQC experiments for recording HN and HC-correlation spectra in proteins at high throughput, J. Biomol. NMR 42 (2) (2008) 129–137, https://doi.org/10.1007/s10858-008-9270-2, URL <https://link.springer.com/article/10.1007/s10858-008-9270-2> .
[10] D. Schulze-Sünninghausen, J. Becker, B. Luy, Rapid heteronuclear single quantum correlation NMR spectra at natural abundance, J. Am. Chem. Soc. 136 (4) (2014) 1242–1245, https://doi.org/10.1021/ja411588d, pMID: 24417402.
[11] L. Frydman, T. Scherf, A. Lupulescu, The acquisition of multidimensional NMR spectra within a single scan, Proc. Nat. Acad. Sci. 99 (25) (2002) 15858–15862, https://doi.org/10.1073/pnas.252644399, URL <https://www.pnas.org/content/99/25/15858.abstract> .
[12] P. Pelupessy, Adiabatic single scan two-dimensional NMR spectrocopy, J. Am. Chem. Soc. 125 (40) (2003) 12345–12350, https://doi.org/10.1021/ja034958g, pMID: 14519020.
[13] Y. Shrot, L. Frydman, Single-scan NMR spectroscopy at arbitrary dimensions, J. Am. Chem. Soc. 125 (37) (2003) 11385–11396, https://doi.org/10.1021/ja0350785, pMID: 16220962.
[14] A. Tal, L. Frydman, Single-scan multidimensional magnetic resonance, Prog. Nucl. Magn. Reson. Spectrosc. 57 (3) (2010) 241–292, https://doi.org/10.1016/j.pnmrs.2010.04.001, URL <https://www.sciencedirect.com/science/article/pii/S0079656510000452> .
[15] P. Giraudeau, L. Frydman, Ultrafast 2D NMR: an emerging tool in analytical spectroscopy, Ann. Rev. Anal. Chem. 7 (1) (2014) 129–161, https://doi.org/10.1146/annurev-anchem-071213-020208, pMID: 25014342.
[16] A. Herrera, E. Fernández-Valle, R. Martínez-Álvarez, D. Molero, Z.D. Pardo, E. Sáez, M. Gal, Real-time monitoring of organic reactions with two-dimensional ultrafast TOCSY NMR spectroscopy, Angew. Chem. Int. Ed. 48 (34) (2009) 6274–6277, https://doi.org/10.1002/anie.200902387, URL <https://onlinelibrary.wiley.com/doi/abs/10.1002/anie.200902387> .
[17] L. Rouger, B. Gouilleux, M. Pourchet-Gellez, J.-N. Dumez, P. Giraudeau, Ultrafast double-quantum NMR spectroscopy with optimized sensitivity for the analysis of mixtures, Analyst 141 (2016) 1686–1692, https://doi.org/10.1039/C6AN00089D.
[18] L. Guduff, I. Kuprov, C. van Heijenoort, J.-N. Dumez, Spatially encoded 2D and 3D diffusion-ordered NMR spectroscopy, Chem. Commun. 53 (2017) 701–704, https://doi.org/10.1039/C6CC09028A.
[19] S. Akoka, P. Giraudeau, Fast hybrid multi-dimensional NMR methods based on ultrafast 2D NMR, Magn. Reson. Chem. 53 (11) (2015) 986–994, https://doi.org/10.1002/mrc.4237, URL <https://onlinelibrary.wiley.com/doi/abs/10.1002/mrc.4237> .

[20] M. Vega-Vazquez, J.C. Cobas, M. Martín-Pastor, Fast multidimensional localized parallel NMR spectroscopy for the analysis of samples, Magn. Reson. Chem. 48 (10) (2010) 749–752, https://doi.org/10.1002/mrc.2659, URL <https://onlinelibrary.wiley.com/doi/abs/10.1002/mrc.2659>.

[21] B. Vitorge, G. Bodenhausen, P. Pelupessy, Speeding up nuclear magnetic resonance spectroscopy by the use of SMAll Recovery Times – SMART NMR, J. Magn. Reson. 207 (1) (2010) 149–152, https://doi.org/10.1016/j.jmr.2010.07.017, URL <https://www.sciencedirect.com/science/article/pii/S1090780710002235> .

[22] P. Schmieder, A.S. Stern, G. Wagner, J.C. Hoch, Application of nonlinear sampling schemes to COSY-type spectra, J. Biomol. NMR 3 (5) (1993) 569–576, https://doi.org/10.1007/BF00174610.

[23] V.A. Mandelshtam, H.S. Taylor, A.J. Shaka, Application of the filter diagonalization method to one- and two-dimensional NMR spectra, J. Magn. Reson. 133 (2) (1998) 304–312, https://doi.org/10.1006/jmre.1998.1476, URL <https://www.sciencedirect.com/science/article/pii/S1090780798914768> .

[24] R. Brüschweiler, F. Zhang, Covariance nuclear magnetic resonance spectroscopy, J. Chem. Phys. 120 (11) (2004) 5253–5260, https://doi.org/10.1063/1.1647054.

[25] Ē. Kupče, R. Freeman, Projection–reconstruction technique for speeding up multidimensional NMR spectroscopy, J. Am. Chem. Soc. 126 (20) (2004) 6429–6440, https://doi.org/10.1021/ja049432q, pMID: 15149240.

[26] D.J. Holland, M.J. Bostock, L.F. Gladden, D. Nietlispach, Fast multidimensional NMR spectroscopy using compressed sensing, Angew. Chem. Int. Ed. 50 (29) (2011) 6548–6551, https://doi.org/10.1002/anie.201100440, URL <https://onlinelibrary.wiley.com/doi/abs/10.1002/anie.201100440> .

[27] V.Y. Orekhov, V.A. Jaravine, Analysis of non-uniformly sampled spectra with multi-dimensional decomposition, Prog. Nucl. Magn. Reson. Spectrosc. 59 (3) (2011) 271–292, https://doi.org/10.1016/j.pnmrs.2011.02.002, URL <https://www.sciencedirect.com/science/article/pii/S0079656511000161> .

[28] P. Schanda, H. Van Melckebeke, B. Brutscher, Speeding up three-dimensional protein NMR experiments to a few minutes, J. Am. Chem. Soc. 128 (28) (2006) 9042–9043, https://doi.org/10.1021/ja062025p, pMID: 16834371.

[29] E. Lescop, P. Schanda, B. Brutscher, A set of BEST triple-resonance experiments for time-optimized protein resonance assignment, J. Magn. Reson. 187 (1) (2007) 163–169, https://doi.org/10.1016/j.jmr.2007.04.002, URL <https://www.sciencedirect.com/science/article/pii/S1090780707001103> .

[30] M. Deschamps, I.D. Campbell, Cooling overall spin temperature: protein NMR experiments optimized for longitudinal relaxation effects, J. Magn. Reson. 178 (2) (2006) 206–211, https://doi.org/10.1016/j.jmr.2005.09.011, URL <https://www.sciencedirect.com/science/article/pii/S1090780705003150> .

[31] Ē. Kupče, R. Freeman, Fast multidimensional NMR by polarization sharing, Magn. Reson. Chem. 45 (1) (2007) 2–4, https://doi.org/10.1002/mrc.1931.

[32] J. Furrer, A. robust, sensitive, and versatile HMBC experiment for rapid structure elucidation by NMR: IMPACT-HMBC, Chem. Commun. 46 (2010) 3396–3398, https://doi.org/10.1039/C000964D, URL <https://pubs.rsc.org/en/content/articlelanding/2010/cc/c000964d> .

[33] D. Schulze-Sünninghausen, J. Becker, M.R.M. Koos, B. Luy, Improvements, extensions, and practical aspects of rapid ASAP-HSQC and ALSOFAST-HSQC pulse sequences for studying small molecules at natural abundance, J. Magn. Reson. 281 (Supplement C) (2017) 151–161, https://doi.org/10.1016/j.jmr.2017.05.012, URL <https://www.sciencedirect.com/science/article/pii/S1090780717301386> .

[34] F. Bloch, Nuclear Induction, Phys. Rev. 70 (1946) 460–474, https://doi.org/10.1103/PhysRev.70.460, URL <https://link.aps.org/doi/10.1103/PhysRev.70.460> .

[35] J.P. Mugler, F.H. Epstein, J.R. Brookeman, Shaping the signal response during the approach to steady state in three-dimensional magnetization-prepared rapid gradient-echo imaging using variable flip angles, Magn. Reson. Med. 28 (2) (1992) 165–185, https://doi.org/10.1002/mrm.1910280202, URL <https://onlinelibrary.wiley.com/doi/abs/10.1002/mrm.1910280202> .

[36] M.K. Stehling, Improved signal in "snapshot" FLASH by variable flip angles, Magn. Reson. Imaging 10 (1) (1992) 165–167, https://doi.org/10.1016/0730-725X(92)90387-F, URL <https://www.sciencedirect.com/science/article/pii/0730725X9290387F> .

[37] K. Nagashima, Optimum pulse flip angles for multi-scan acquisition of hyperpolarized NMR and MRI, J. Magn. Reson. 190 (2) (2008) 183–188, https://doi.org/10.1016/j.jmr.2007.10.011, URL <https://www.sciencedirect.com/science/article/pii/S1090780707003333?via%3Dihub> .

[38] Y. Xing, G.D. Reed, J.M. Pauly, A.B. Kerr, P.E.Z. Larson, Optimal variable flip angle schemes for dynamic acquisition of exchanging hyperpolarized substrates, J. Magn. Reson. 234 (0) (2013) 75–81, https://doi.org/10.1016/j.jmr.2013.06.003, URL <https://www.sciencedirect.com/science/article/pii/S1090780713001419> .

[39] S. Ehni, B. Luy, A systematic approach for optimizing the robustness of pulse sequence elements with respect to couplings, offsets, and B_1-field inhomogeneities (COB), Magn. Reson. Chem. 50 (2012) 63–72, https://doi.org/10.1002/mrc.3846.

[40] S. Ehni, B. Luy, Robust INEPT and refocused INEPT transfer with compensation of a wide range of couplings, offsets, and B_1-field inhomogeneities (COB3), J. Magn. Reson. 247 (2014) 111–117, https://doi.org/10.1016/j.jmr.2014.07.010, URL <https://www.sciencedirect.com/science/article/pii/S1090780714002109> .

[41] C. Zwahlen, P. Legault, S.J.F. Vincent, J. Greenblatt, R. Konrat, L.E. Kay, Methods for measurement of intermolecular NOEs by multinuclear NMR spectroscopy: application to a bacteriophage λ N-peptide/boxB RNA complex, J. Am. Chem. Soc. 119 (29) (1997) 6711–6721, https://doi.org/10.1021/ja970224q.

[42] A.J. Shaka, C.J. Lee, A. Pines, Iterative schemes for bilinear operators; application to spin decoupling, J. Magn. Reson. (1969) 77 (2) (1988) 274–293, https://doi.org/10.1016/0022-2364(88)90178-3, URL <https://www.sciencedirect.com/science/article/pii/0022236488901783> .

[43] M. Kadkhodaie, O. Rivas, M. Tan, A. Mohebbi, A.J. Shaka, Broadband homonuclear cross polarization using flip-flop spectroscopy, J. Magn. Reson. (1969) 91 (2) (1991) 437–443, https://doi.org/10.1016/0022-2364(91)90210-K, URL <https://www.sciencedirect.com/science/article/pii/002223649190210K> .

[44] F. Kramer, W. Peti, C. Griesinger, S.J. Glaser, Optimized homonuclear Carr–Purcell-type dipolar mixing sequence, J. Magn. Reson. 149 (1) (2001) 58–66, https://doi.org/10.1006/jmre.2000.2271, URL <https://www.sciencedirect.com/science/article/pii/S1090780700922717> .

[45] J. Furrer, F. Kramer, J.P. Marino, S.J. Glaser, B. Luy, Homonuclear Hartmann-Hahn transfer with reduced relaxation losses by use of the MOCCA-XY16 multiple pulse sequence, J. Magn. Reson. 166 (1) (2004) 39–46, https://doi.org/10.1016/j.jmr.2003.09.013, URL <https://www.sciencedirect.com/science/article/pii/S1090780703003355>.

[46] J. Becker, B. Luy, CLIP–ASAP-HSQC for fast and accurate extraction of one-bond couplings from isotropic and partially aligned molecules, Magn. Reson. Chem. 53 (11) (2015) 878–885, https://doi.org/10.1002/mrc.4276, URL <https://onlinelibrary.wiley.com/doi/abs/10.1002/mrc.4276> .

[47] A.G. Palmer, J. Cavanagh, P.E. Wright, M. Rance, Sensitivity improvement in proton-detected two-dimensional heteronuclear correlation NMR spectroscopy, J. Magn. Reson. (1969) 93 (1) (1991) 151–170, https://doi.org/10.1016/0022-2364(91)90036-S, URL <https://www.sciencedirect.com/science/article/pii/002223649190036S> .

[48] L.E. Kay, P. Keifer, T. Saarinen, Pure absorption gradient enhanced heteronuclear single quantum correlation spectroscopy with improved sensitivity, J. Am. Chem. Soc. 114 (26) (1992) 10663–10665, https://doi.org/10.1021/ja00052a088.

[49] C.J. Turner, P.J. Connolly, A.S. Stern, Artifacts in sensitivity-enhanced HSQC, J. Magn. Reson. 137 (1) (1999) 281–284, https://doi.org/10.1006/jmre.1998.1692, URL <http://www.sciencedirect.com/science/article/pii/S1090780798916925> .

[50] F.A.A. Mulder, R. Otten, R.M. Scheek, Origin and removal of mixed-phase artifacts in gradient sensitivity enhanced heteronuclear single quantum correlation spectra, J. Biomol. NMR 51 (1) (2011) 199–207, https://doi.org/10.1007/s10858-011-9554-9, URL <https://link.springer.com/article/10.1007/s10858-011-9554-9> .

[51] M. Garwood, Y. Ke, Symmetric pulses to induce arbitrary flip angles with compensation for rf inhomogeneity and resonance offsets, J. Magn. Reson. (1969) 94 (3) (1991) 511–525, https://doi.org/10.1016/0022-2364(91)90137-I, URL <https://www.sciencedirect.com/science/article/pii/002223649190137I> .

[52] Ē. Kupče, R. Freeman, Wideband excitation with polychromatic pulses, J. Magn. Reson. Ser. A 108 (2) (1994) 268–273, https://doi.org/10.1006/jmra.1994.1123, URL <https://www.sciencedirect.com/science/article/pii/S1064185884711235> .

[53] M.R.M. Koos, H. Feyrer, B. Luy, Broadband excitation pulses with variable RF amplitude-dependent flip angle (RADFA), Magn. Reson. Chem. 53 (11) (2015) 886–893, https://doi.org/10.1002/mrc.4297.

[54] M.R.M. Koos, H. Feyrer, B. Luy, Broadband RF-amplitude-dependent flip angle pulses with linear phase slope, Magn. Reson. Chem. 55 (9) (2017) 797–803, https://doi.org/10.1002/mrc.4593, mrc.459.

[55] G.C. Chingas, A.N. Garroway, R.D. Bertrand, W.B. Moniz, Zero quantum NMR in the rotating frame: J cross polarization in AX_N systems, J. Chem. Phys. 74 (1) (1981) 127–156, https://doi.org/10.1063/1.440866.

[56] L. Braunschweiler, R.R. Ernst, Coherence transfer by isotropic mixing: application to proton correlation spectroscopy, J. Magn. Reson. (1969) 53 (3) (1983) 521–528, https://doi.org/10.1016/0022-2364(83)90226-3, URL <https://www.sciencedirect.com/science/article/pii/0022236483902263> .

[57] N. Chandrakumar, G.V. Visalakshi, D. Ramaswamy, S. Subramanian, Analysis of collective modes in some A_MX_N systems, J. Magn. Reson. (1969) 67 (2) (1986) 307–318, https://doi.org/10.1016/0022-2364(86)90435-X, URL <https://www.sciencedirect.com/science/article/pii/002223648690435X> .

[58] O. Schedletzky, S.J. Glaser, Analytical coherence-transfer functions for the general AMX spin system under isotropic mixing, J. Magn. Reson. Ser. A 123 (2) (1996) 174–180, https://doi.org/10.1006/jmra.1996.0232, URL <https://www.sciencedirect.com/science/article/pii/S1064185896902326> .

[59] H.M. Pastawski, G. Usaj, P.R. Levstein, Quantum interference phenomena in the local polarization dynamics of mesoscopic systems: an NMR observation, Chem. Phys. Lett. 261 (3) (1996) 329–334, https://doi.org/10.1016/0009-2614(96)00978-5, URL <https://www.sciencedirect.com/science/article/pii/0009261496009785> .

[60] A. Majumdar, Analytical expressions for isotropic mixing in three- and four-spin topologies in $^{1}3C$ systems, J. Magn. Reson. Ser. A 121 (2) (1996) 121–126, https://doi.org/10.1006/jmra.1996.0151, URL <https://www.sciencedirect.com/science/article/pii/S1064185896901515> .

[61] Z.L. Mádi, B. Brutscher, T. Schulte-Herbrüggen, R. Brüschweiler, R.R. Ernst, Time-resolved observation of spin waves in a linear chain of nuclear spins, Chem. Phys. Lett. 268 (3) (1997) 300–305, https://doi.org/10.1016/S0009-2614(97)00194-2, URL <https://www.sciencedirect.com/science/article/pii/S0009261497001942> .

[62] O. Schedletzky, B. Luy, S.J. Glaser, Analytical polarization and coherence transfer functions for three coupled spins 1/2 under planar mixing conditions, J. Magn. Reson. 130 (1) (1998) 27–32, https://doi.org/10.1006/jmre.1997.1274, URL <https://www.sciencedirect.com/science/article/pii/S109078079791274X> .

[63] B. Luy, O. Schedletzky, S.J. Glaser, Analytical polarization transfer functions for four coupled spins $\frac{1}{2}$ under isotropic mixing conditions, J. Magn. Reson. 138 (1) (1999) 19–27, https://doi.org/10.1006/jmre.1998.1702, URL <https://www.sciencedirect.com/science/article/pii/S1090780798917025> .

[64] B. Luy, S.J. Glaser, Analytical polarization and coherence transfer functions for three dipolar coupled spins $\frac{1}{2}$, J. Magn. Reson. 142 (2) (2000) 280–287, https://doi.org/10.1006/jmre.1999.1938, URL <https://www.sciencedirect.com/science/article/pii/S1090780799919389> .

[65] B. Luy, S.J. Glaser, Negative polarization transfer between a spin 1/2 and a spin 1, Chem. Phys. Lett. 323 (5) (2000) 377–381, https://doi.org/10.1016/S0009-2614(00)00549-2, URL <https://www.sciencedirect.com/science/article/pii/S0009261400005492> .

[66] B. Luy, S.J. Glaser, Analytical planar mixing transfer functions for two coupled spin-1 nuclei, J. Magn. Reson. 153 (2) (2001) 210–214, https://doi.org/10.1006/jmre.2001.2438, URL <https://www.sciencedirect.com/science/article/pii/S1090780701924383> .

[67] Burkhard Luy, Steffen J. Glaser, Superposition of scalar and residual dipolar couplings: analytical transfer functions for three spins 1/2 under cylindrical mixing conditions, J. Magn. Reson. 148 (1) (2001) 169–181, https://doi.org/10.1006/jmre.2000.2194, URL <https://www.sciencedirect.com/science/article/pii/S1090780700921943> .

[68] B. Luy, S.J. Glaser, Transverse magnetization transfer under planar mixing conditions in spin systems consisting of three coupled spins 1/2, J. Magn. Reson. 164 (2) (2003) 304–309, https://doi.org/10.1016/S1090-7807(03)00251-9, URL <https://www.sciencedirect.com/science/article/pii/S1090780703002519> .

[69] I. Solomon, Relaxation processes in a system of two spins, Phys. Rev. 99 (1955) 559–565, https://doi.org/10.1103/PhysRev.99.559, URL <https://link.aps.org/doi/10.1103/PhysRev.99.559> .

[70] R. Freeman, H.D.W. Hill, B.L. Tomlinson, L.D. Hall, Dipolar contribution to NMR spin-lattice relaxation of protons, J. Chem. Phys. 61 (11) (1974) 4466–4473, https://doi.org/10.1063/1.1681764, URL <https://scitation.aip.org/content/aip/journal/jcp/61/11/10.1063/1.1681764> .

[71] N. Niccolai, M.P. de Leon de Miles, S.P. Hehir, W.A. Gibbons, Correlation time measurements of amino acid side chains from proton selective spin-lattice relaxation rates, J. Am. Chem. Soc. 100 (20) (1978) 6528–6529, https://doi.org/10.1021/ja00488a058.